UNIL | Université de Lausanne
Faculté des géosciences
et de l'environnement

Master of Science in Geography

Subglacial channel characterisation using high-resolution remote-sensing methods and modelling on the Haut Glacier d'Arolla, Switzerland

Sébastien Ruttimann

Under the direction of Prof. Stuart Lane
Dr. James Irving

Expert Prof. Grégoire Mariéthoz

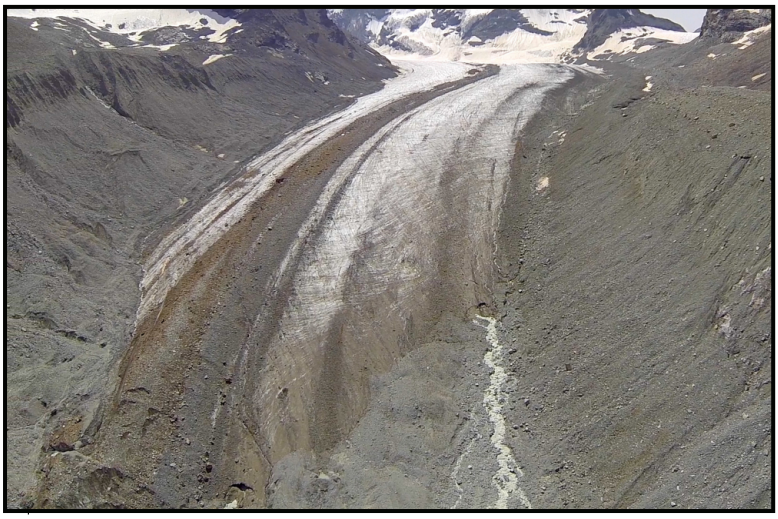

Maîtrise universitaire ès sciences en géographie | Janvier - 2016

Cover picture
Drone view of the Haut Glacier d'Arolla (08.08.14)

Foreword

This memoire is divided into three sections and one annex, written around a scientific paper. The first part contains a general introduction to subglacial research. It is followed by a summary of the main objectives of the work, the methods, and justification of the field site. The second part contains the scientific article addressing the combination of ground-penetrating radar and drone photogrammetry in order to detect a near-snout subglacial channel, assess its geometry, and perform flow and sediment transport modelling. The third part discusses the potential and limits of the methods as well as perspectives for future research. Finally, more details on the ground-penetrating radar survey and processing steps are available in the Annex. In this context, overlap between the different parts is likely so as to guarantee the correct structure of the scientific paper alongside a more general introduction and conclusion.

Acknowledgements

This work would not have been possible without the support of a large number of people. I would like to thank in particular:

- Prof. Stuart Lane, for transmitting his passion for glaciology and alpine environments, for his invaluable help on the field and in modelling, and for his guidance throughout this work.
- Dr. James Irving, for sharing his enthusiasm for geophysics methods, for his particular expertise with the ground-penetrating radar on the field, in data processing and forward modelling.
- Dr. Ludovic Baron, for his priceless help using and combining equipment on the field.
- PhD Student Chrystelle Gabbud, for her fervent interest in this work, the time spent sharing opinions and data, and giving numerous wise advices.
- The people at ETH Zurich – Institut für Geophysik, especially Dr. Lasse Rabenstein and Christoph Bärlocher, for the time spent and their trust in lending us their GPR equipment for several weeks.
- Philippe Hertig, Claude Hertig and Sophie Ruttimann, for reviewing this work numerous times, for their various advices and encouragement.
- Sandrine Folly, Hervé Ruttimann, Kate Lane, for their assistance on the field.
- The Air Glacier Helicopter Company, for their availability, transport capacities and amazing pilots' skills.
- The IDYST and ISTE Institutes for providing high-quality equipment and software.
- And all those who gave me a hand, advice, or contributed to this work.

Thank you very much

Summary

Glaciers have a major impact on mountain catchment hydrology by storing water in cold periods and releasing it during warm periods, as well as transporting considerable amounts of eroded material. Understanding how meltwater flows through glaciers is key to understanding glacier dynamics and its results in effects such as speedup events and bed lubrication. The primary objective of this study was to use high-resolution ground-penetrating radar to detect subglacial channels on the Haut Glacier d'Arolla. The key question is whether or not ground-penetrating radar techniques can be used to identify and to estimate the geometry of a subglacial channel and to what extent; and what the data obtained tell us about subglacial flow and sediment transport processes.

The results have provided insight into the characteristics of a major near-snout subglacial channel. The channel was followed for 20 m upglacier and evidence suggested that the conduit was significantly larger than expected and rapidly became smaller as the overlying ice thickens. Flow modelling revealed that the channel could never be full of water as compared with discharge records, confirming other field reports of near-snout atmospheric channel flow (e.g. Hooke, 1984). Evidence from ground-penetrating radar, drone photogrammetry, and flow and sediment modelling suggested a combination of sediment clogging and flushing mechanics coupled with bed and ice-wall concentrated erosion to be the driving factors of observed channel dimensions. Sediment clogging and flushing could be of great influence for water pressure dynamics and glacier speedup events, leading to new research questions in relation to subglacial hydrology.

Key words

glacier hydrology, subglacial drainage, ground-penetrating radar, sensors and software pulseEkko Pro, digital drone photogrammetry, orthoimagery, digital elevation model (DEM)

Résumé

Les glaciers ont un impact majeur sur l'hydrologie des bassins versants de montagne de par leur rôle de stockage d'eau en période froide, la relâchant pendant les périodes chaudes, et emportant par la même occasion des quantités considérables de matériaux érodés. Comprendre comment l'eau de fonte se comporte à travers les glaciers est un élément clé pour appréhender le fonctionnement des dynamiques glaciaires et leurs conséquences. L'objectif principal de cette étude est d'utiliser des techniques de télédétection de haute résolution afin de détecter des chenaux sous-glaciaires dans le Haut Glacier d'Arolla. Le point clé étant de savoir si le ground-penetrating radar (géoradar de haute résolution) peut être utilisé pour identifier et déduire la géométrie d'un chenal sous-glaciaire, et ce que les informations obtenues permettent de déduire sur les processus d'écoulements et de transport sous-glaciaire.

Les résultats ont permis de déterminer certaines caractéristiques d'un chenal sous-glaciaire proche du front du Haut Glacier d'Arolla. Le chenal a pu être suivi sur environ 20 m et les données suggèrent qu'il serait bien plus large qu'attendu, devenant rapidement plus bas avec l'accroissement de l'épaisseur de glace. La modélisation de l'écoulement de l'eau a démontré que le chenal ne peut jamais être rempli d'eau selon les débits mesurés par Grande Dixence S.A., confirmant ainsi d'autres observations d'écoulement à pression atmosphérique dans la zone préfrontale (ex : Hooke, 1984). Les résultats du ground-penetrating radar, de la photogrammétrie par drone et des modélisations d'écoulement et transport sédimentaire suggèrent une combinaison de mécanismes d'obstruction et de vidange du chenal, couplés avec une concentration de l'érosion sur ses bords, comme étant le facteur principal expliquant les dimensions du chenal observé. Le blocage du chenal par les sédiments et la vidange sont supposés influencer de manière importante les épisodes d'augmentation de la pression dans le système de drainage et les événements d'élévation du glacier et d'accélération de la vitesse d'écoulement ; ce qui laisse envisager de nouvelles orientations et questions de recherche dans le domaine de l'hydrologie sous-glaciaire.

Mots clés

hydrologie glaciaire, drainage sous-glaciaire, ground-penetrating radar, géoradar, sensors and software pulseEkko Pro, photogrammétrie par drone, orthoimagerie, modèle numérique de terrain (MNT)

Part I – Introduction

Part II - Article: Subglacial channel characterisation using high-resolution remote-sensing methods and modelling on the Haut Glacier d'Arolla, Switzerland

Part III - Conclusions

Part IV - Annex I and references

Part I - Introduction

Chapter picture
The Mont Collon and the proglacial area of the Haut Glacier d'Arolla (top picture, 07.31.14)
Bottom picture : Glacier du Mont Collon and Petit Mont Collon (08.04.14)

1. Glacier hydrology

Glaciers have a major impact on climate, hydrology and geomorphic processes. Ice fields – often partially covered by snow – have a high albedo and interact with the atmosphere by sending back solar energy contributing to the world climate equilibrium (Hock, 2005). Glaciers also play a water storage role during cold periods, releasing it in warm periods with an important influence on the hydrology of mountain catchments. Glaciers finally influence the landscape through erosion and deposition processes as suggested by both erosional and depositional landforms.

Understanding snow and ice melting mechanisms and how meltwater flows through glaciers are key elements to understanding glacial dynamics. It has been suggested that increasing water levels in subglacial drainage systems can speed up ice flows by lubricating the ice bed contact (Björnsson, 1998; Mair, Sharp et Willis, 2002; Mair et al., 2003). Changes in the subglacial drainage system related to the season and amount of water have been suggested: an inefficient distributed system appears at the end of winter; increasing meltwater through the summer transforms the system into a more efficient channelled one (Nienow, Sharp et Willis, 1998) (Fig. 1.1). As subglacial drainage systems are generally inaccessible, indirect methods such as dye-tracing were the main tools for these studies and allowed estimation of key flow parameters. However the usage of tracers is prone to uncertainties and breakthrough curves can be disturbed by various factors such as channel roughness (Gulley et al., 2012b; Gulley et al., 2013). Thus the transition between distributed system and channelized system has been questioned in recent studies on cold and polythermal glaciers (Gulley et al., 2012b; Gulley et al., 2013) emphasising the need for further research in quantifying the actual morphology of subglacial channel systems.

1.1 Subglacial drainage theories

With current understanding, a distributed drainage system is assumed to be present at the end of winter when flow is at a minimum and ice closure effects are dominant (Kamb, 1987). This system is characterized by a large number of small-interconnected inefficient channels (Mair et al., 2003). With the beginning of summer, increased water supply is thought to destabilize the distributed system, increasing water pressure (Fountain and Walder, 1998), and sliding speeds, and ultimately creating a network of pathways constituted by major channels with larger hydraulic capacities (Fig. 1.1), which has the effect of decreasing water pressure (Nienow et al., 1998) and sliding speeds (Mair et al., 2002). This transition within the glacier has been shown to closely follow the snow-ice interface as snowmelt water infiltrates the glacier through moulins and ice cracks and increases the discharge (Nienow et al., 1998), subglacial pressure, and hence melt.

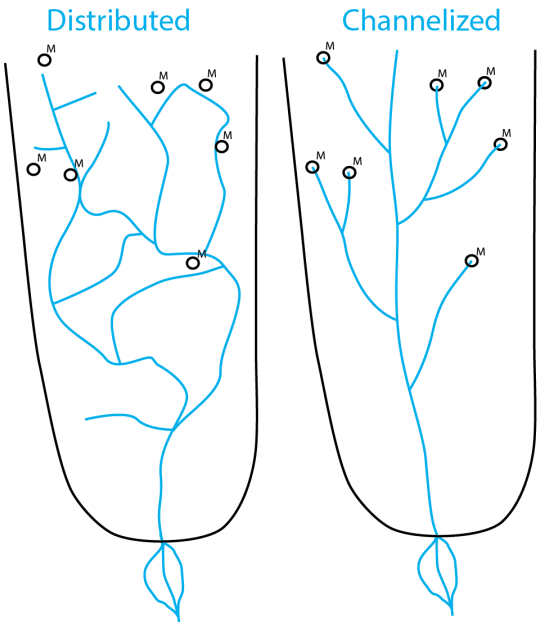

Figure 1.1: Diagram of a distributed drainage system thought to be present at the end of winter. Channelized system is thought to appear with increasing discharge from ice melting. Channels are generally thought to start at moulins (M) as suggested by Gulley et al. (2012a).

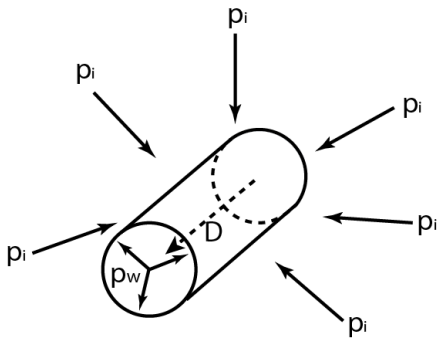

Figure 1.2: Röthlisberger channel. Discharge (D) water pressure (ρ_w) keeps the channel open, ice pressure (ρ_i) tends to close it. Modified from Walder 2010.

However the exact timing of the shift and the geometrical characteristics of the evolving channel system are still debated. A number of types of drainage morphology have been suggested for the distributed system: thin water layers at the bed surface (Weertman, 1983), links between cavities (Lliboutry, 1968), flow through subglacial sediment pores (Engelhardt et al., 1978), small channels with a few cm radius (Walder and Fowler, 1994). For the channelized shape other morphologies were also suggested: Röthlisberger R-channels (Röthlisberger, 1972), Nye Channels (Nye, 1972) and horizontal-elliptic channels (Hubbard and Nienow, 1997).

Röthlisberger (1972) demonstrated numerically that R-channels should reflect a balance between creep closure and channel enlargement (Hubbard and Nienow, 1997) and as a result should be circular when surrounded by ice (Fig. 1.2) and semi-circular when running on the glacier bed, incising upward in the ice (Fig. 1.7b). Field observations (Hooke, 1984) have shown that at least two other shapes could exist: Hooke (Hooke et al., 1988; Hooke et al., 1990) reported that channels could be broad

and low instead of semi-circular on the basis of dye-tracer and borehole investigations. Channels have also been reported to be thin and vertically elongated (e.g. Stuart et al., 2003). Hooke (1984) data showed that channels were not permanently water filled, thus melting would be concentrated on the channel walls instead of the channel's ceiling (Hooke, 1984; Cutler, 1998). Concentrated melting in the channel walls would either create low and broad shapes, or vertically elongated shapes by rapid bed erosion.

Ceiling creep closure may also be faster than lateral wall closure because bedrock friction slows down lateral ice creep closure. Similarly Fountain (1993) found in a dye-tracer study at South Cascade Glacier (USA) broad and sinuous channels instead of the theoretically expected straight semi-circular shape. Extending Hooke's conclusions, Cutler (1998) found that channel shape might evolve over the melt season: from semi-circular early in the melt season to a flatter shape as season advances (Cuffey and Paterson, 2010). He also suggested that channels would not be water filled during cold periods and at night.

$$\Phi = \rho_w\, g\, z + c\, [\rho_i\, g\, (H - z)]$$

Equation 1.1: Adapted Shreve (1972) hydraulic potential from Willis et al. (2009)

In an attempt to reconstruct drainage patterns theoretically, Shreve (1972) suggested a flow model based on the physical principle that in every hydraulic system, water should flow from zones of high hydraulic potential to zones of lower hydraulic potential, developing a formula to determine the hydraulic potential at every point in a glacier using water and ice density, gravity, ice thickness, water pressure and altitude (Equation 1.1). The Shreve (1972) model says that subglacial channels should cross hydraulic potential contours at right angles given the following assumptions: (i) homogeneous and isotropic permeability; (ii) uniformly distributed recharge; (iii) constant water pressure in the channels; (iv) conduit enlargement and creep closure rate is the same for the whole glacier. Even though these assumptions are probably never met on actual glaciers, the Shreve (1972) model has produced convincing drainage reconstructions on some glaciers such as the Haut Glacier d'Arolla (Sharp et al., 1993) and has been widely used in recent years (e.g. Pälli et al., 2003; Fig 1.3a and 1.3b).

The uniform recharge assumption is possibly one of the most problematic: water inputs from basal melting (1-100 mm a^{-1}) are of very different magnitude than punctual water inputs from moulins (1000-10000 mm a^{-1}), which in turn could have a major impact on the subglacial water pressure distribution and channel position (Gulley et al., 2012a). The Shreve model would thus be incorrect and channels may not be concentrated near the central line of the glacier but should begin at the bottom of moulins and crevasses (Gulley et al., 2012a). Furthermore it was demonstrated that higher pressure could be attained in channels than in a distributed system (Hubbard et al., 1995; Mair et al., 2003) and that pressure varies through time. Observations have shown that higher pressure in subglacial channels results in stronger uplift and higher glacier flow speeds over the channels (Gordon et al., 1998; Mair et al., 2003) but the uplift remains localized. On the contrary, the distributed system is more spatially spread out resulting in larger areas affected by uplift but slower flow speeds.

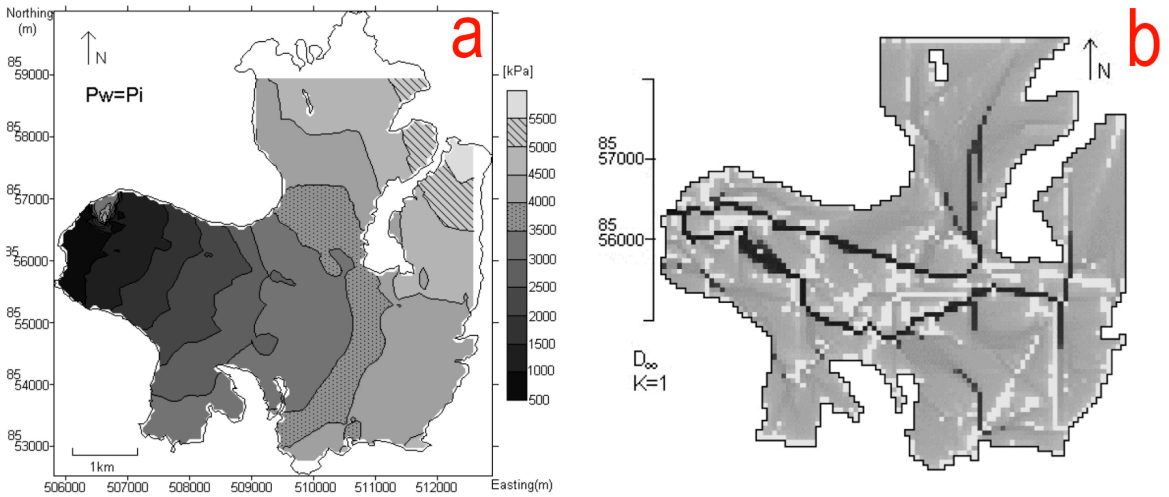

Figure 1.3: (a) map of the hydraulic potential for a water pressure equal to ice pressure ($p_w = p_i$) using Shreve (1972) equation. (b) subglacial flow model using calculated hydraulic potentials. (Pälli et al., 2003. Werenskioldbreen Glacier, Svalbard).

Recent studies (e.g. Gulley et al., 2012b) have shown a link between daily flow speed variations and dye-tracer dispersivity at a moulin above a well-established channel. Dye-tracers are of particular utility to infer numerous parameters in inaccessible environments, such as the connection between input location and sampling location, travel speed estimation using return time, complexity of the flow path using the dispersivity, section area and roughness estimation. Daily variations observed by Gulley et al. (2012b) are of the same order-of-magnitude as the ones observed when the drainage system is shifting from distributed to channelized: dispersivity is low during the day when melting is high, conversely melting is lower at night and dispersivity is high. These findings show that the amount of water in the channels modifies the return curves of dye-tracer concentration through time (breakthrough curves or BTCs) even though the actual channel geometry hasn't changed and therefore changes all inferences on channel geometry, storage time in moulins, time of shift between distributed and channelized system, etc. (Gulley et al., 2012a; Gulley et al., 2012b; Gulley et al., 2013).

Gulley et al. (2012b) argued that high levels of dispersivity in BTCs may actually be explained by channel bed roughness variations and not necessarily by channel geometry changes, for example: a low flow depth and a bed characterized by large boulders (high roughness) will increase the flow tortuosity, creating complex velocity fields and thus decreasing flow speeds and producing BTCs response similar to that of a distributed system. Conversely when water level increases, the tortuosity of flow decreases as boulders become covered by water and moved by transport, flow speed increases, creating BTCs that look like those of a channelized system (Gulley et al. 2012b; Gulley et al., 2013). Furthermore, as flow depths change on seasonal and daily scales, BTCs may indicate changes in the subglacial system morphology when there have been none. Consequently low flow speed and high dispersivity are not sufficient to establish that there has been a change in the drainage system configuration. So, breakthrough curves may not be a good diagnostic of the kind of subglacial drainage system present at the glacier bed.

Nonetheless, long dye-tracer travel times from early-in-the-melt-season moulin injections have commonly been interpreted to demonstrate the presence of a distributed system (Fig. 1.4, Injection 1). Dye-tracers injected in boreholes early in the

melt season and far from any channel by Gordon et al. (1998) showed travel times of days, even weeks instead of hours like moulins-injections (Fig. 1.4, injection1). As suggested by Gulley et al. (2012b), it is more likely that injection into moulins delivered dye into a channel network that had persisted through winter, but where the channels had closed partially (Fig. 1.5, Benn et al., 2009; Gulley et al., 2012b). It is also likely that channels form earlier in the melt season than previously thought (Gulley et al., 2012b). Thus, if flow is not channelized even early in the melt season, BTCs from moulins injections should be similar to borehole injections anywhere on the glacier under the widespread distributed system assumption.

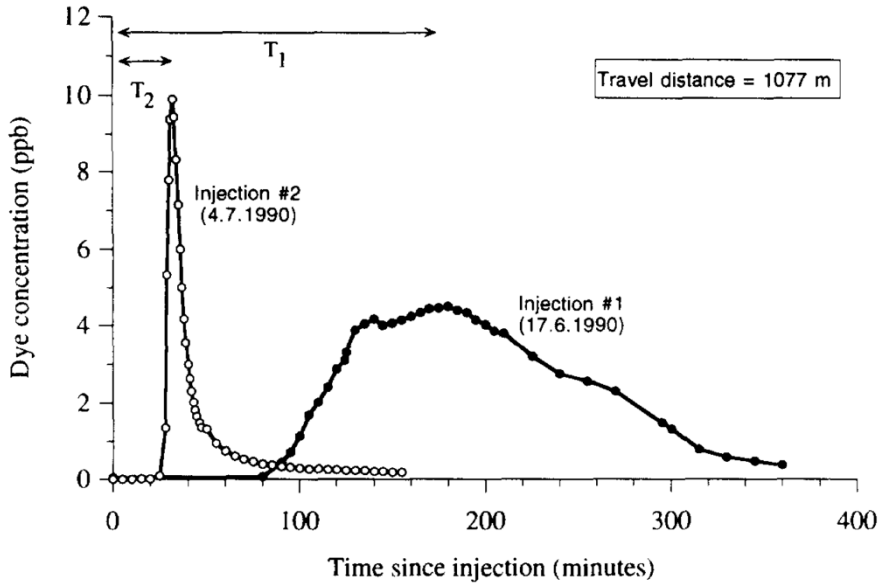

Figure 1.4: Two typical breakthrough curves. Injection 1 has a high dispersivity and is therefore taken as a distributed drainage system response, this is however questioned by Gulley et al. (2012b) as distributed drainage response should be in days or even weeks. Injection 2 has a high concentration peak taken as a channelized drainage system (Hubbard and Nienow, 1997).

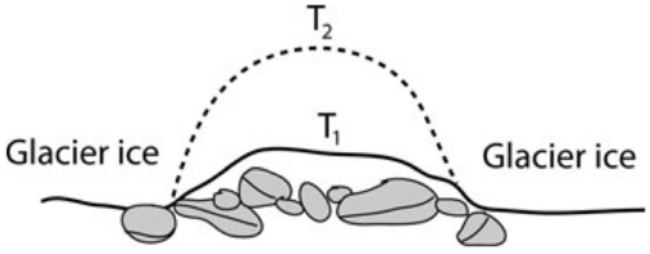

Figure 1.5: Channels might persist during winter but in much smaller form. Early season meltwater flow speeds are considerably decreased by bed roughness due to the low water level (T_1). BTCs would have a high dispersivity and could be interpreted as a sign of a distributed drainage system. (Gulley et al., 2012b)

Following Figure 1.5, it is possible that the distributed-channelized channel systems also evolve by erosion and filling of their bed, rather than solely ice melting and ice closure mechanisms, something that has been overlooked by many. Bed erosion and deposition may be a more rapid process than ice melting, thus possibly having greater impact on subglacial system evolution. Indeed, incision into underlying till was noted by Gulley et al. (2013) while discussing consequences for flow roughness parameterization.

1.2 General objectives and methodological approach

Given the above, this mémoire has two primary objectives. The first was to focus on the usage of ground-penetrating radar (GPR) to detect and infer the position and geometry of a subglacial channel, in order to better understand the evolution of near snout channels, reflecting the above review: most of our understanding of the morphodynamics of subglacial channels has come from indirect inference using BTCs; there are many fewer direct measurements of subglacial channel morphology. Ground-penetrating radar methods were chosen for their portability, non-intrusiveness, rapid data acquisition and for the excellent resolution and considerable depth that can be attained, if used correctly, especially on electrically resistive materials such as ice. GPR has been widely used in glaciology especially to measure ice thickness (Rippin et al., 2003; Sharp et al., 1993; Welch et al., 1998; Willis et al., 2009), internal structures (Irvine-Finn et al., 2006), map the ice-bedrock interface (King et al., 2008) and investigate subglacial hydrology (Murray et al., 2000; Stuart et al., 2003; Vincent et al., 2012).

The second objective of this work was to use this information to interpret the implications of the measured subglacial channel geometries for existing understanding of near-snout subglacial hydrology. Key here was to consider not only ice-related melt and closure processes, but also sediment bed dynamics. We know that coarse bed sediment transport by water is a nonlinear function of the excess of bed shear stress over a critical value, the bed shear stress itself a function of discharge (e.g. Nitsche et al., 2011). Thus, it is highly unlikely that coarse bed sediment transport is continuous. If it is discontinuous, then there should be bed sediment erosion and deposition over a number of timescales (hourly, daily, weekly) as a function of changing transport capacity and upstream sediment supply. Thus, near snout channels (as well as, potentially, more distal channels) should be morphodynamic. This process is not at all well known.

1.3 Field site choice and justification

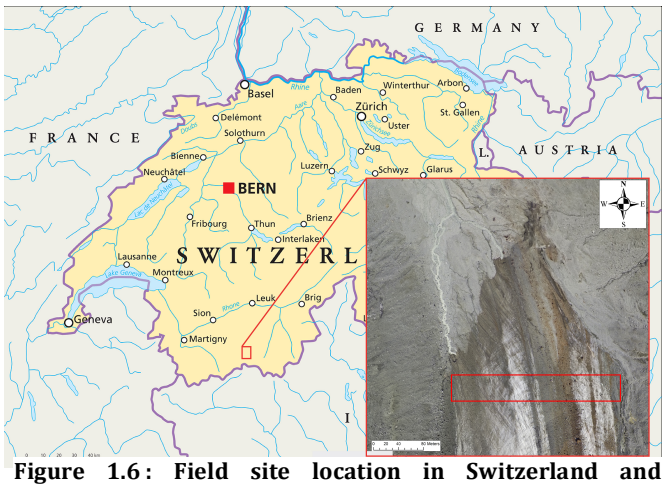

Figure 1.6: Field site location in Switzerland and highlighted GPR survey area on the Haut Glacier d'Arolla (2014 orthophoto).

The Haut Glacier d'Arolla is located at the southern end of the Val d'Hérens in south-west Switzerland (Fig. 1.6 and 1.7a). It is a temperate valley glacier with one main tongue flowing northward, fed by two separate firn basins. During the summer of 2014 and 2015, the glacier was drained by two subglacial streams uniting to create the Borgne d'Arolla (Fig. 1.8a), whose water is extracted by a Grande Dixence SA water intake further downstream.

The Haut Glacier d'Arolla is a well-adapted site for GPR surveys mainly because of the small number of crevasses and the relatively flat tongue with few large obstacles and large topographic variations (Fig. 1.7a, Fig. 1.8). The Haut Glacier d'Arolla has been extensively studied since the 1990s, in particular the characterization of the subglacial drainage system and its temporal evolution (Sharp et al., 1993; Nienow et al., 1996; Nienow et al., 1998). Studies have shown an evolution of the drainage system from distributed to channelized over the course of the melt season (Nienow et al., 1998), leading to a system dominated by two main channels (Sharp et al., 1993). Large pressure amplitudes on a daily scale have also been observed in the channelized system (Swift et al., 2005b; Hubbard et al., 1995).

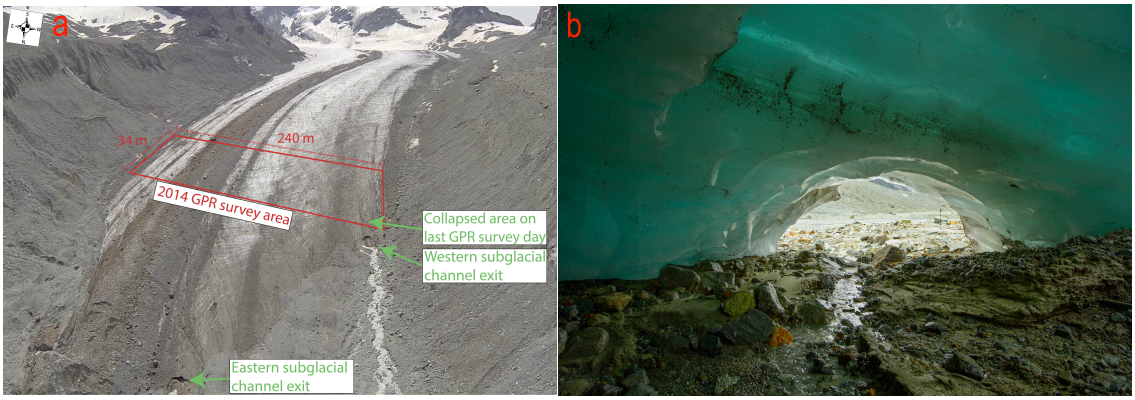

Figure 1.7: Aerial view of the Haut Glacier d'Arolla (a) and remains of a subglacial channel exit with a typical Röthlisberger shape (b) (Personal pictures, August 2014).

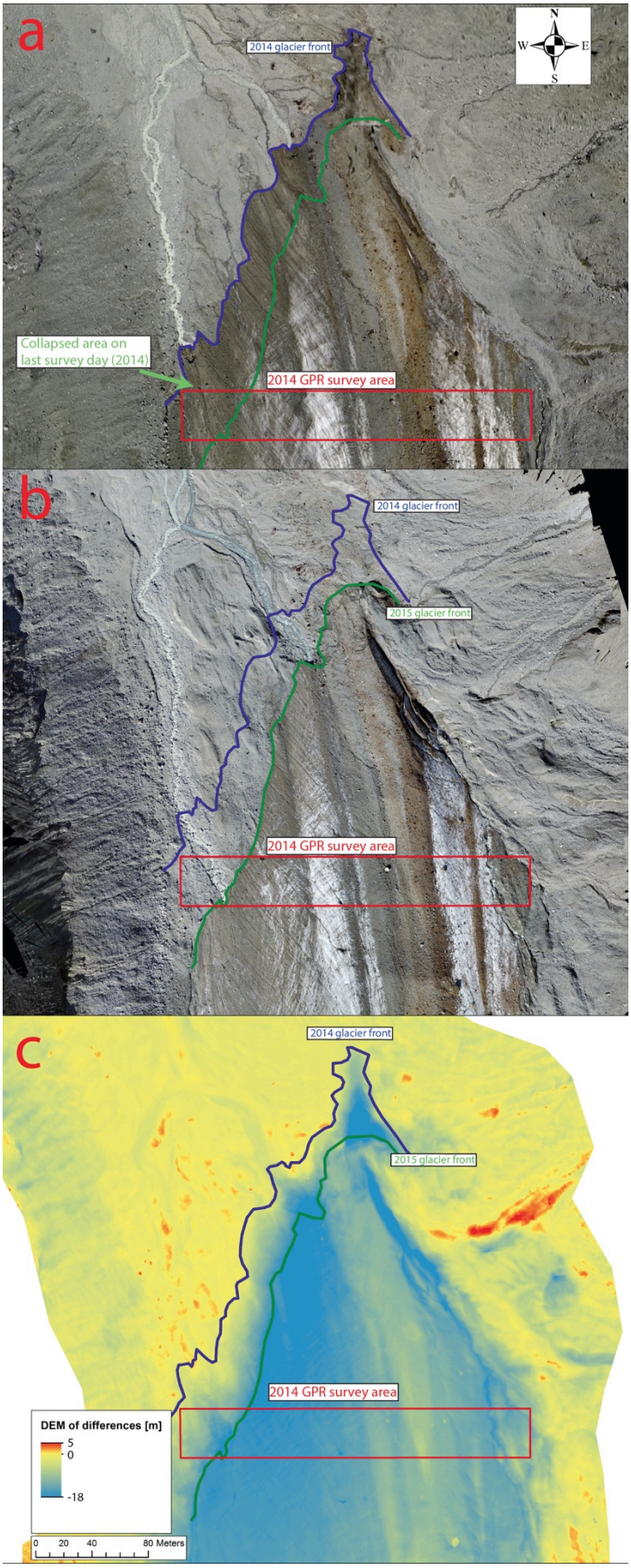

Figure 1.8: August 2014 (a) and September 2015 (b) drone orthophotos. Extensive glacier retreat (70 m) has left part of GPR survey area free of ice, allowing for 2015 western channel riverbed topography extraction.

2014 orthophoto (a) was constructed using a DJI Phantom 2 equipped with a GoPro3 camera. Quality is therefore lower (lower GSD and many artefacts) than 2015 orthophoto (b), which was created using a DJI Inspire1 drone (4k camera). 2014 flight path was also not optimized for a photogrammetry study, hence bad data quality. DEM of differences (c) reveals important glacier melting in both glacier extent and glacier surface. Both channel exits are marked by strong altitudes differences due to extensive channel roof collapsing and melting.

The DEM of differences (c) also reveal important modifications in the Sandur area as braided streams appear to have changed their course and carved new channels in the sediments while creating deposits in abandoned channels. The eastern glacier flank also shows substantial deposition of material coming from up glacier and from the 1850's moraine.

Part II - Article

Chapter picture
Stuart and Sandrine performing a GPR survey on the Haut Glacier d'Arolla (top picture, 08.04.14)

Typical Röthlisberger channel shape in the snout of the Haut Glacier d'Arolla (bottom picture, 08.08.14)

2. Subglacial channel characterisation using high-resolution remote-sensing methods and modelling on the Haut Glacier d'Arolla, Switzerland

2.1 Introduction

The subglacial drainage system is thought to influence the sliding speed of glaciers by lubricating the glacier base and reducing basal drag (Willis, 1995 ; Björnsson, 1998 ; Mair, Sharp et Willis, 2002; Mair et al., 2003). Under current understanding, a distributed drainage system is assumed to be present at the end of winter when flow is at a minimum (Kamb, 1987). This system is characterized by a large number of small-interconnected and inefficient channels (Mair et al., 2003). During summer, intensifying water supply is thought to increase the water pressure (Fountain and Walder, 1998), thereby increasing the sliding speed and, through melting, creating a network of pathways (a distributed system) eventually evolving into major channels with larger hydraulic capacities (channelized system). Shifts between distributed and channelized flow are thought to lead to decreasing subglacial water pressure (Nienow et al., 1998) and sliding speed (Mair et al., 2002). The transition between distributed and channelized systems beneath the glacier has been shown to closely follow the snow-ice interface line as snowmelt water infiltrates the glacier through moulins and ice cracks and increases the magnitude of peak discharge (Nienow et al., 1998).

The drainage morphology of the distributed system has been described as a thin water layer at the bed surface (Weertman, 1983), links between cavities (Lliboutry, 1968), flow through subglacial sediment pores (Engelhardt, Harrison and Kamb, 1978) and small channels with mm to cm radius (Walder and Fowler, 1994). For the channelized shape; Röthlisberger R-channel (Röthlisberger, 1972) and Nye Channel (Nye, 1972) theories have stood the test of time even though modified by data collected since 1972 (Walder, 2010). Originally subglacial R-channels were thought to be circular within the glacier and semi-circular on the glacier bed (Röthlisberger, 1972). Channel shapes were thought to reflect a balance between creep closure and channel enlargement by ice melt (Hubbard and Nienow, 1997). Field observations have shown that at least two other shapes exist. Hooke (Hooke et al., 1988; Hooke et al., 1990) reported that channels may be broad and low instead of semi-circular on the basis of dye-tracer and borehole investigations and other reports showed that englacial channels could also be vertically elongated (e.g. Stuart et al., 2003). Hooke (1984) suggested that channels are not permanently water-filled, thus melting is concentrated on the walls instead of the channel's ceiling, creating a low and broad shape. Ceiling creep closure is also faster than lateral wall closure because the bedrock friction slows down ice creep closure. Similarly Fountain (1993) reported, for a dye-tracer study at South Cascade Glacier (USA), broad and sinuous channels instead of the theoretically expected straight semi-circular shape. Extending Hooke's conclusions, Cutler (1998) found that channel shape might evolve over the melt season: from semicircular early in the melt season to a more laterally-elongated shape as season advances (Cuffey and Paterson, 2010). He also suggested that channels would not be water filled during cold periods and at night.

In order to evaluate englacial channel geometry, Stuart et al. (2003) used ground-penetrating radar (GPR) to analyse a 900 m long channel on a cold glacier using reflection strength, travel-time information and the reflection coefficient (polarity). Strong reflections were expected from englacial water. The reflection coefficient was used to differentiate ice-air, ice-water and air-water boundaries. The analysed data allowed the authors to infer the channel depth, height, water content and width; the channel started as semi-circular at the base of a moulin and became vertically elongated near the outlet. Hooke (1984) suggested that melting of channel walls is faster than creep closure, thus channels are most likely to be at atmospheric pressure beneath thin ice and englacial channels would become vertical by rapid bed erosion (also observed by Stuart et al., 2003). These studies suggest that subglacial and englacial channels can adopt a wide variety of morphologies resulting from multiple processes (Gulley et al., 2012a). It was recently shown (Gulley et al., 2012b; Gulley et al., 2013) that channel bed conditions and dynamics may have a significant impact on water flow. Given the high sediment production rates of Alpine glaciated basins, it is probable that there is significant sediment accumulation at the glacier bed. We know that sediment transport by rivers is a non-linear function of the excess of flow shear stress, and hence discharge, over a critical value (e.g. Nitsche et al., 2011). Due to diurnal melt cycles, as well as the effects of specific rain storm events, coarse sediment transport capacity in subglacial channels is likely to be discontinuous. The inevitable consequence of this discontinuity will be erosion and deposition within subglacial channels over a variety of timescales, with a rate that may be much more important than the rates of ice-related melt or creep processes. This latter process has yet to be quantified.

The aim of this paper is, with a focus on the near snout zone, to quantify the morphology of subglacial channels and to begin to interpret what this means for our understanding of subglacial hydrology. This is achieved through the combination of ground-penetrating radar (GPR), basic flow and sediment transport modelling, and photogrammetry based remote sensing. We begin by reporting on 60 GPR survey lines conducted near the snout of the Haut Glacier d'Arolla, Switzerland in the summer of 2014. A large subglacial channel was detected and followed for 20 m upglacier. Our results suggest that the channel is broad and low rather than semicircular and becomes flatter as the ice thickens upglacier. Comparing GPR extracted channel bed with photogrammetric scans performed a year later over the deglaciated channel show significant variations in channel bed morphology over time. Next, using the extracted channel geometry, we show substantial sediment erosion and deposition in-between surveyed sections. Finally, based on these observation, we propose the hypothesis of a sediment driven mechanism controlling the channel morphodynamics.

2.2 Field site

Figure 2.1 : Field site location in Switzerland and highlighted GPR survey area on the Haut Glacier d'Arolla (2014 orthophoto).

The Haut Glacier d'Arolla is a temperate valley glacier located at the head of Val d'Hérens, Valais, Switzerland (Fig. 2.1). Two separate firn basins feed the main glacier tongue, which flows north for approximately 2 km and is 800 m wide. The western firn basin goes up to 3300 m.a.s.l., whereas the eastern basin goes up to 3500 m.a.s.l. The glacier snout is located at around 2570 m and its total area is about 4 km^2 with maximum ice thickness of 160 m. The glacier is in a phase of severe retreat (25 m/year) (Zryd, 2001).

A large number of studies on glacial hydrology have been conducted on this glacier since the 1990s, in particular the characterization of the subglacial drainage system and its temporal evolution (Sharp et al., 1993; Nienow et al., 1996; Nienow et al., 1998). These studies have suggested that the system is dominated by two main channels (Sharp et al., 1993) evolving from distributed to channelized over the course of the melt season (Nienow et al., 1998). The channelized drainage system is also thought to be characterized by large pressure amplitude changes on a daily scale due to the interactions with an extensive distributed system feeding larger channels (Swift et al., 2005b; Hubbard et al., 1995).

Section I: Subglacial channel detection and geometry assessment

2.3.1 Methodology

2.3.1.1 Ground-penetrating radar measurements

In August 2014, GPR measurements were conducted close to the glacier snout (Fig. 2.2a). This location allowed a priori estimation of subglacial channel position under the survey region. During the last days of measurement, a large crack began to appear on the lowest survey line over the channel. The channel collapsed on the final day (Fig. 2.2b), where it was seen to have a width of approximately 10 m.

The GPR measurements were conducted using a Sensors & Software pulseEkko Pro GPR system attached to a custom built support, allowing one person to carry both 100 Mhz antennas at a constant 1 m offset with a dGPS rover in the backpack. Trace stacking was set to 8 as a compromise between data quality and the number of traces collected per second. A 2 m spacing between survey-lines on the north-south axis was used. A total of 60 survey lines were performed including: (i) 7 glacier wide profiles; (ii) 12 on the glacier's central moraine where the eastern subglacial channel was thought to be; (iii) 25 profiles more focused on the western subglacial channel for 20 m upglacier; and (iv) two lines repeated every 30 minutes over the course of one day above the subglacial channel to test for GPR measurement reliability (16 lines).

Data processing included: (1) RTK positioning error corrections; and then (2) standard GPR data processing: first, the GPR data were dewow-ed to remove superimposed low-frequency transients using a residual median filter method (window of 35 in this case). Second, the data were gained to compensate rapid signal attenuation with depth using a smooth gain function raising the time vector to a power of 1.1. Third, smoothing was applied to soften staircasing effects in the dGPS recorded traces coordinates, traces were subsequently grouped together using binning method (bins of 0.25 m) and shifted to account for variations in topography. Fourth, principal component analysis filtering to remove very predictable noise by subtracting reconstructed data set to original data (first 5 principal components were used). Fifth, F-K migration to correct mispositioning of reflectors and modifications of observed depth by refocusing scattered waves to their correct locations. Migration velocities were determined for each profile by fitting diffraction hyperbolas. Finally, manual picking to pull out features for 3D visualization and further analysis was executed. More detailed explanations of each processing steps and the data acquisition procedure are available in Annex I. The output of this stage was, for each cross-glacier GPR survey line, a detailed image of the glacier bed, the ice surface and possible subglacial channels.

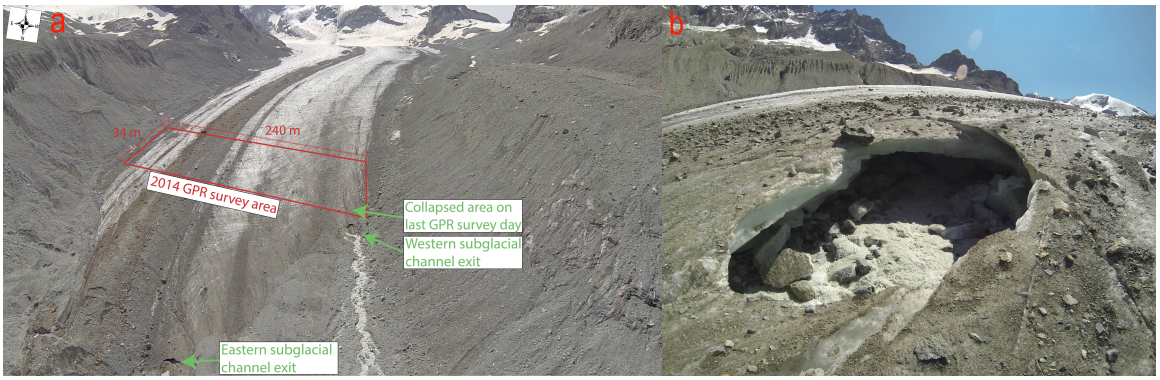

Figure 2.2 : Survey locations and important features (a). Collapsed channel on August 12th 2014 (b). Two subglacial channel exits are visible at the snout of the Haut Glacier d'Arolla and are thought to each drain one side of the glacier basin (Personal pictures, August 2014).

2.3.1.2 Data evaluation

The application of GPR to subglacial channel quantification carries with it the possibility of the misinterpretation of GPR signals. Thus, we included explicitly in the analysis a number of tests to establish the reliability of our data. First, two potential pitfalls have to be avoided with radar monitoring of subglacial hydrological processes (Kulessa et al., 2008): rapid temporal changes in; (a) radar attenuation by the near surface ice water content; and (b) subglacial reflectivity, the second pitfall potentially leading to serious misinterpretations of the subglacial structures. Notably, profiles may be severely affected by increasing water content in the near glacier surface during the day. To test for such pitfalls, repeated measurements were performed over the course of one day at a fixed time interval.

Second, forward modelling was used to grow the confidence that we can have in our interpretations. Ground penetrating radar wave speeds are determined by the material's electrical properties, most notably the dielectric permittivity, and are required for proper representation in terms of depth rather than 2-way travel time. To migrate our filed data we assumed a constant velocity in the subsurface and wave speeds were

determined from diffraction hyperbolas. However GPR waves travel faster in the air than in the ice, and faster in the ice than in water. As subsurface feature depth locations are based on return time in GPR profiles, shift phenomena may occur when waves cross materials having different wave speeds. Therefore, features such as the channel bed are improperly migrated due to channel air content "pulling upwards" underlying features. Water content produces the opposite effect.
To quantify these errors, calculations were performed using 2D Finite-difference time-domain (FDTD) reflection GPR modelling codes (Irving and Knight, 2006), allowing estimation of the effects induced by permittivity and conductivity differences between materials such as ice, air and water, and also allowing deduction of the impact of the applied data processing by comparing an initial model of the subsurface and the resulting GPR image after processing.

The general channel section geometry was reproduced in two-dimensional space using common permittivity/conductivity values for air (ε_r= 1; σ = 0 mS/m), ice (ε_r= 4; σ = $1*10^{-5}$ mS/m) and till (ε_r= 6; σ = $1*10^{-3}$ mS/m) to create a model of the subsurface containing an air-filled subglacial channel (12 m wide by 3 m high) over a till bed, and under shallow ice depth (10 m). This configuration is different from reality, as the channel did actually contain a small amount of water running at its bed (as shown in Fig. 2.2b) but the representation was used as a compromise between modelling, calculations and interpretation complexity.

2.3.1.3 Closure modelling

Following the geometry assessment, error determination and geometry corrections, calculations were performed using the Hooke (1984) equation to determine the probable rates of channel closure in the survey area. Channel shapes are the result of two processes: deformation by ice creep closure and enlargement by water induced ice melting. An equilibrium state is reached when channels are full of water (Röthlisberger, 1972) and most creep closure happens during winter when there is no water. However, channels near the snout are thought not to be full of water (Hooke, 1984) so creep closure from the roof should happen all year round. To evaluate the extent of creep closure on the detected channel, we applied a simple calculation following Hooke (1984), which approximates the closure rate dr/dt of a semi-circular channel at atmospheric pressure (Equation 2.1).

$$\frac{dr}{dt} = \left(\frac{\rho_i g h}{n_2 A_2}\right)^{n_2} r$$

Equation 2.1: Closure rate of a semi-circular channel at atmospheric pressure (Hooke, 1984)

Where p_i is the ice density, g is gravitational acceleration, h is the ice thickness, n_2 = 3 and A_2 = $5.8*10^7$ are constants from Glen's flow law assuming homogeneous isotropic ice, r is the radius of the channel.

2.3.1.4 Photogrammetry

Drone photogrammetry was performed on the glacier snout in August 2014 using a DJI Phantom2 drone equipped with a GoPro Hero3, and in September 2015 with a DJI Inspire1 drone. Both flights were performed with manual controls, using FPV monitors to frame the shots. The GoPro camera was set up to capture an image every 2 seconds, while the Inspire1 camera was controlled manually from the remote control also with a two seconds frame rate in mind to ensure sufficient frontal overlap. Flight altitudes were situated around 50 m above the take-off area, and back-and-forth flight lines were used to ensure sufficient sides overlap. Black and white targets were placed in the survey area as ground control points in 2015 and were measured using a Trimble dGPS system in the CH1903 LV03 coordinate system. The resulting pictures were then processed using Pix4D software to produce point clouds, densified point clouds, orthomosaics and Digital Elevation Models (DEMs). Each ground control point target location was manually marked on approximately 20 pictures to rectify the 2015 point cloud. The 2014 point cloud was subsequently rectified using comparable features in both point clouds (2015 and 2014) such as large boulders in areas that were thought to be stable. Following rectification, the DEM resolution for the 2015 scan was 3.3 cm and 27 cm for 2014.

The September 2015 drone survey revealed that the glacier had retreated 70 meters on its western side and the 2014 GPR survey area was mostly free of ice, allowing for river-bed profile extractions at the position of the GPR profiles for comparison.

Both beds were subsequently reconstructed by interpolating the topography between the ten sections on a 0.5 m grid. Subtracting the 2015 bed by the 2014 GPR bed provided altitudinal differences for each cell of the grid and sedimentary budget (m^3) was estimated for each cell by multiplying the altitudinal difference with the width (0.5 m) and length (0.5 m) of each cell. Summing the cells value at the location of each GPR section provided its estimated sedimentary budget (Table 2.1, p. 35).

2.3.2 Results

2.3.2.1 Measurement reliability

Repeated measurements

The repeated measurements performed over the course of one day at a fixed time interval of 30 minutes (Fig. 2.3) suggested that increasing ringing effects were the main factor of change between morning and afternoon profiles. But no severe changes that would lead to serious misinterpretations were observed, especially given the thin ice layer over the subglacial channel. Thus, the results are not thought to have been affected by water content variation throughout the day to the extent that they would prevent further analysis. Changes in the channel ceiling are however noticeable (Fig. 2.3(iii) and (iv)) and may be sources of uncertainties in further calculations. They are, however, thought to lead to only a few centimetres of error.

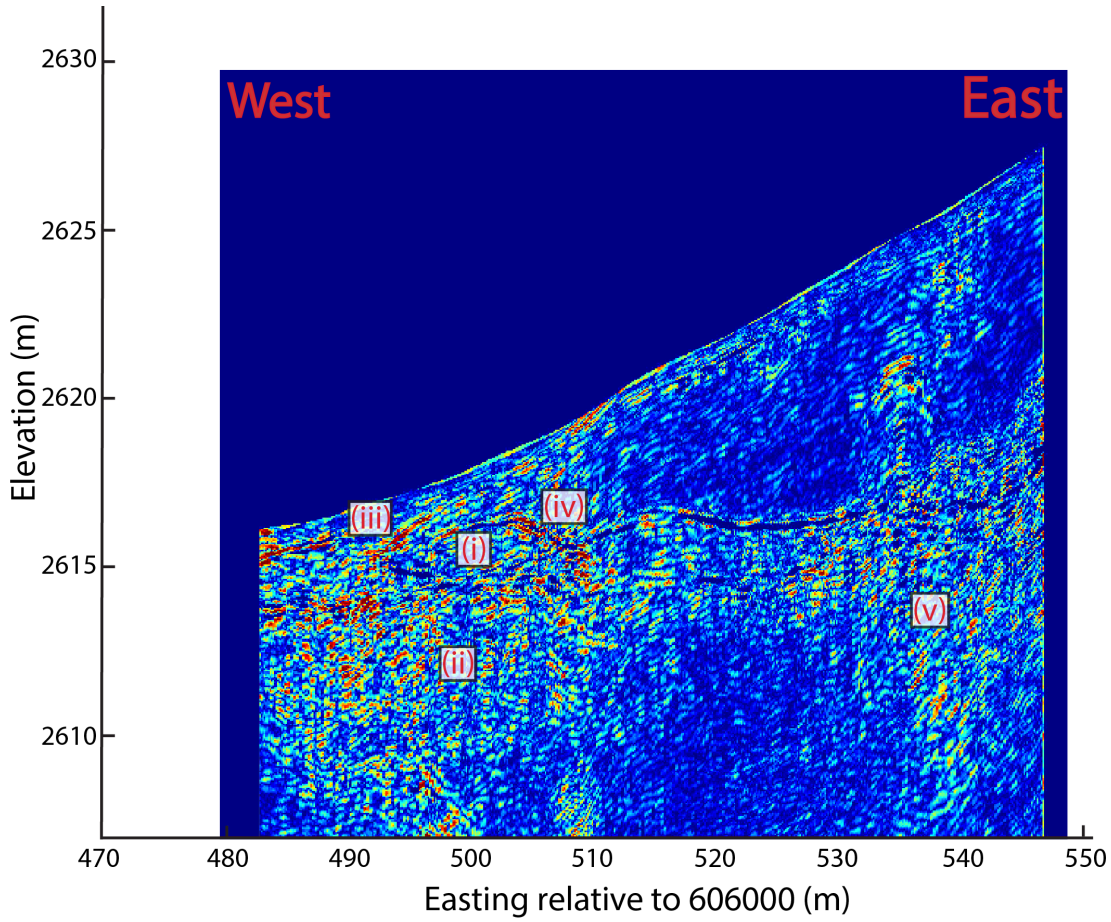

Figure 2.3 : Difference image between two repeated survey lines (10 :30 am and 2 pm) over the subglacial channel (i), mainly demonstrating changes due to increased ringing effects following water content increase throughout the day (ii and v). While probably limited to a few centimetre deviations, some changes are notable on the channel ceiling (iii and iv) and may be sources of uncertainties.

Forward GPR modelling

In order to gain confidence in the interpretations, the forward GPR modelling sought to address the effects of the constant wave speed assumption used in data processing. The model of the subsurface (Fig. 2.4a) was used with FDTD reflection modelling and the synthetic GPR data were then processed using the same assumptions as the field data (Fig. 2.4b).

Resulting simulated and processed data showed variable accuracy in representing subsurface structures (comparison of yellow dots in Fig. 2.4a and 2.4b). In perfect conditions (no scatterers and homogeneous ice), the position of the channel roof and the surrounding bedrock are precise to the scale of centimetres, however the channel bed is mis-positioned by a much higher factor (described below) due to air in the channel (Fig. 2.4b, blue outline), which significantly increases radar wave speeds. As migration is based here on average radar wave speeds in the ice, such deformation will not be corrected.

A simple calculation using radar wave speeds in the air (0.3 m/ns), and in the ice (~0.15 m/ns), suggests a pull up phenomenon of ~half the true height of the channel under an air containing cavity. In Fig. 2.4b the measured channel centre height in the resulting GPR image is 1.4 m. Using a factor 2 ($\frac{0.3}{0.15}$ m/ns), the true channel bed position in the centre of Fig. 2.4 is therefore (10.4+(1.4*2)) = 13.2 m which is very close to the model of the subsurface (13.5 m). Performing the calculation at several points (Fig. 2.4b, green dots) of the channel allows reconstruction of a more accurate bed position (dashed green line in Fig. 2.4b). The same correction can be applied to the bed reflector in the Haut Glacier d'Arolla profiles. The current correction does not however take into account a water layer in the channel, but assumes the channel is filled with air. This assumption was used as a compromised between modelling and result interpretation complexity, and also because the exact amount of water and the granulometry in the channel at the time of measurement were unknown. This simplification is however a source of uncertainty in our calculations.

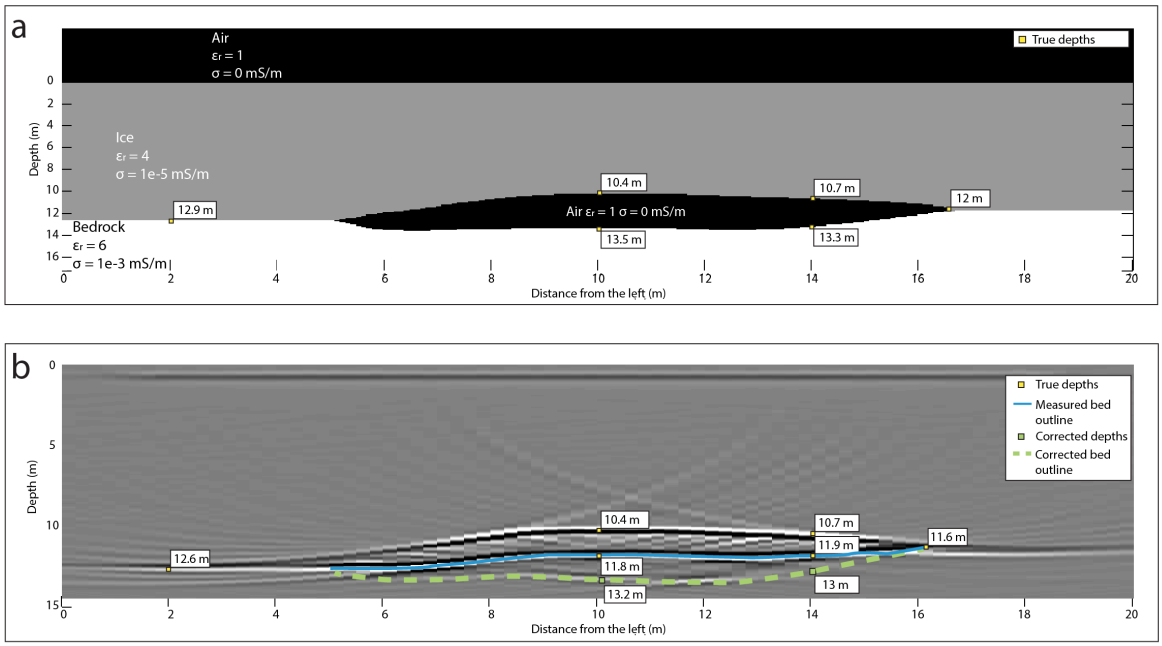

Figure 2.4 : Permittivity model of the subsurface (a) and result after simulation (b), processed using dewow, gain, binning and migration. Result (b) shows good accuracy on the channel roof and surrounding bedrock, however channel air content accelerates radar waves, shifting the channel bed position upward (b, blue outline). Applying a factor 2 based correction allows reconstruction of a more accurate bed position (b, dashed green line)

2.3.2.2 Ground-penetrating radar measurements

Ground-penetrating radar surveys produced clear profiles (Figure 2.5) allowing the glacier bed (ice-till contact) to be seen (Fig. 2.5a, (v)) and a semi-circular shape near the glacier bed on the left (west) part under shallow ice depth (Fig. 2.5a, (i)). This semi-circular shape is interpreted as a major subglacial channel and its roof is signalled by a strong ice-air reflector (Fig. 2.5b, light blue outline), which appears to have a polarity similar to the direct pulse (hereafter noted positive polarity). Inside the channel a second strong and mostly flat reflector is noticeable (Fig. 2.5b, blue outline), and is interpreted as a mixed reflector between the channel bed and water level due to what appears to be an inverse polarity to the direct pulse (noted negative polarity). In the currently used antenna connection configuration, the ice-air boundary reflection coefficient at normal incidence is positive and thus should produce positive polarity reflectors marked on the Fig. 2.5a and 2.5b by black-white-black lines. Air-water and air-till reflection coefficient are negative and thus should produce negative polarity marked on Fig. 2.5a and 2.5b by white-black-white.

Near the centre of the channel, the reflector appears to be much stronger and could be the sign of water running on the bed. A third less visible reflector can sometimes be seen below the mixed bed-water reflector. Uncertainties are however high on this reflector's origin, it may very well be the product of ringing effects, out of plane scatterers or the result of migration focusing. Surrounding the channel, the ice-till contact is unusually strongly marked on some profiles (Fig. 2.5b), which could likely be caused by the presence of a thin water layer running alongside the channel in a distributed system.

The eastern drainage channel was expected to be near the glacier centre according to previous Shreve potential calculations (Sharp et al., 1993), but the profiles did not reveal clear signs of its presence, except for two unusually strong reflectors and ringing effects at the bedrock lowest point (Fig. 2.5a, (ii) and (iii)), possibly suggesting the presence of a water-containing cavity. The left-side reflector (Fig. 2.5a, (ii)) even shows a possible wide semi-circular shape, which may reflect the position of the main eastern drainage channel. The possible negative polarity reflector might be the sign of an ice-water reflector (Fig. 2.5a, (ii)), thus suggesting the presence of one, to two water-filled subglacial channels. However no further evidence is available to prove this hypothesis and these reflectors may also be the result of migration artefacts. No further analyses were performed here.

Interestingly, the GPR profiles revealed a "radar transparent layer" in the first 5 to 10 m overlaying the upper radar scatterer layer (Fig. 2.5a, (v)). Randomly distributed scatterers compose the radar scattering layer in the Haut Glacier d'Arolla producing radar profiles typical of temperate ice (Brown, Harper and Bradford, 2009; Bamber, 1987; Odegard et al., 1996). On the contrary, very few to almost no reflectors are present in the transparent layer. The zone was confirmed not to be the result of either migration or filtering because it is already visible after simple gain of the data. Its presence was also confirmed in summer 2015 when new ground-penetrating radar surveys were conducted in the same area with a different GPR instrument (unpublished data).

Our GPR profiles allowed the observation of the evolution of the western subglacial channel as it changes shape between each profile but remains consistently wide and thin varying between 20 m and 13 m (Fig. 2.6). Interestingly the channel seems to become flatter and narrower upglacier as the ice thickens (Fig. 2.6 and 2.7).

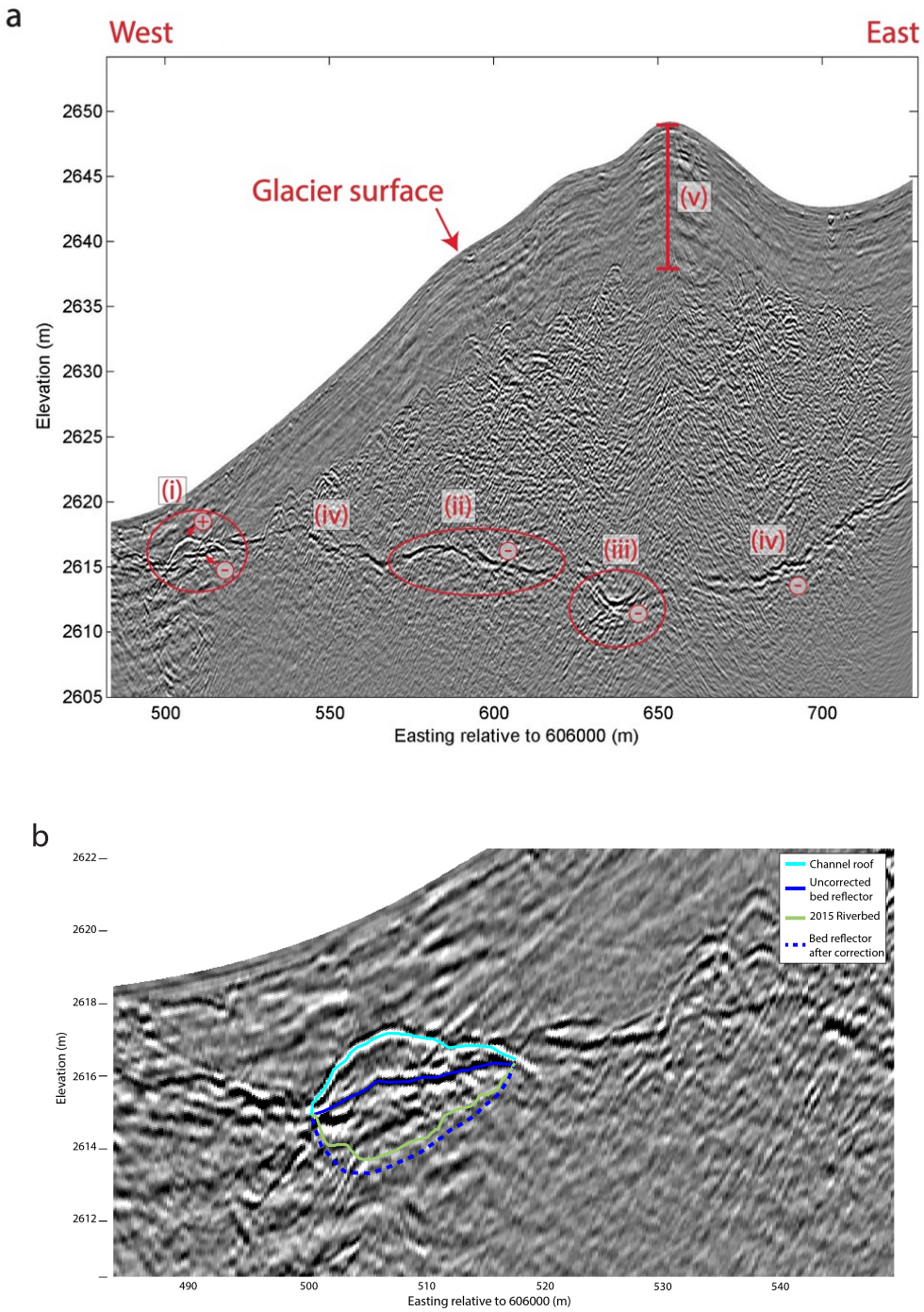

Figure 2.5 : Annotated glacier wide surveys with important features (2.5a) and zoom on the subglacial channel (2.5b). The western-most subglacial channel roof is clearly marked by a strong positive reflector (2.5b, light blue line) and the bed reflector (blue line) follows the roof shape due to the air content of the channel, which increases wave velocities. Dotted blue line (2.5b) represents the channel bed after correcting for air-layer induced waves acceleration, which follows closely the 2015 photogrammetry extracted riverbed (2.5b, green line). Ringing effects can be observed below the channel (2.5b). Near the centre of 2.5a, two strong reflectors can be seen (2.5a, (ii) and (iii)). They are assumed to reflect the position of one or more glacier drainage channels as the reflector resembles the semi-circular shape of a channel roof and polarity suggests for water containing cavities or wet till. Strong ringing effects and migration artefacts also mark the bed lowest point (2.5a, (iii)). In the first 5 to 10 meters of ice from the surface (2.5a, (v)), a region with less to almost no scatterers is visible and appears to be similar to cold layer of polythermal glaciers (radar transparent layer).

2.3.2.3 Channel geometry and closure

Regarding the channel geometry, the ten sections in Fig. 2.6 are of consistent width, but become flatter up-glacier. Interestingly significant upstream-downstream variation can be observed in the geometry, certain sections being larger or deeper than others, possibly resulting in areas of slower water flow and fill whilst other would be prone to downward incision. This is particularly visible while looking at the slope variation between the 2014 bed and comparing with 2015 riverbed (Fig. 2.6): deeper sections seem to be more inclined to deposition while shallower sections show incision. It also appears the downward incision has been limited to preferential areas especially in sections 1 and 2 (Fig 2.6 and Table 2.1).

Comparing the GPR extracted channel bed profiles with DEM extracted river bed profiles shows good agreement with lateral channel extent on most GPR profiles (Fig. 2.6) and eventual direct observations of the collapsed area confirmed the presence of a subglacial channel containing a low water level running on a till bed. After correcting for wave speed acceleration in the air (see Forward modelling), the mixed bed-water reflector closely follows the extracted 2015 riverbed in certain sections (Fig. 2.6, section 5 and 8), while other sections showed substantial downward incision (Fig. 2.6, sections 1, 2, 4, and Table 2.1) or conversely substantial channel fill (Fig. 2.6, sections 3, 7, 8, 10 and Table 2.1), suggesting strong channel bed evolution between the 2014 GPR measurements and the 2015 photogrammetry measurements, with a bias towards incision upstream and fill downstream. It is however important to note that the bed position correction accuracy is likely to be low as it is derived from numerous assumptions such as wave speeds in the ice, unknown out of plane scatterers affecting wave speed, the processing applied to the data. However, calculations of approximate sediment budget per section were performed (Table 2.1) and confirm significant deposition (positive budgets) on certain sections, while others show slight negative budgets.

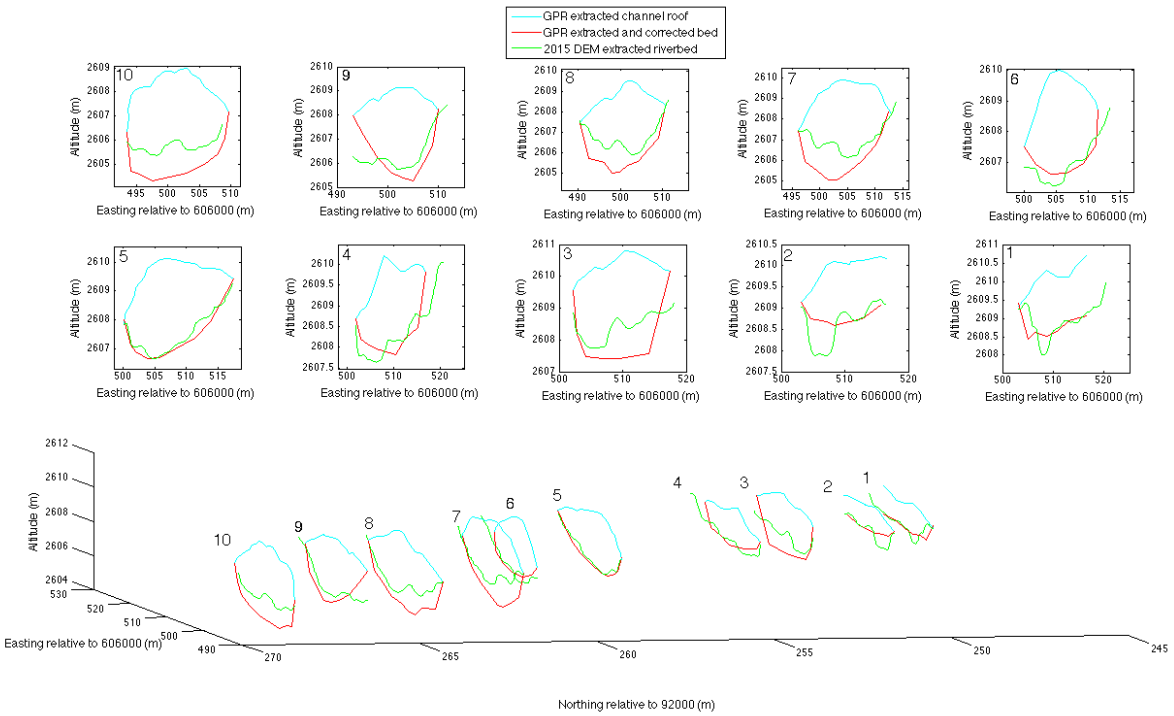

Figure 2.6 : Extracted channel sections geometry from the 2014 ground-penetrating radar survey, with corrected bed position for channel air-content wave acceleration. Comparison with 2015 riverbed sections demonstrated bed variations with substantial downward incision on certain sections (sections 1, 2, 4), substantial deposition (sections 3, 7, 8, 10). Uncertainties are however high concerning the applied channel bed correction as it derives from numerous assumptions.

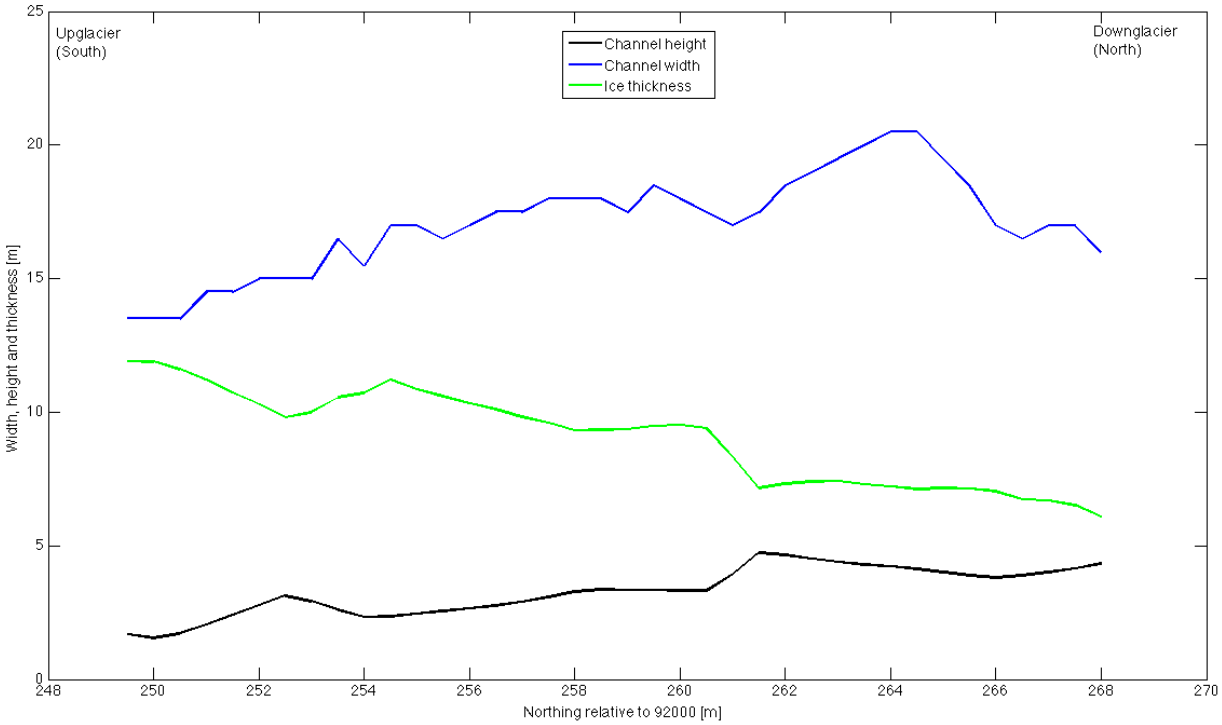

Figure 2.7: Plot demonstrating the western channel width and height evolution under the 20 m of survey area as extracted and corrected from 2014 GPR sections data. The evolution of the channel height appears to be negatively linked with the ice thickness above it and seems to become lower upglacier (south), decreasing from 3 m to 1.6 m. Similarly, the channel width appears to follow the same trend as it first increases then decreases upglacier but still remaining particularly wide from 21 m to 13.5 m. Such trend is thought not to be the result of systematic processing and picking errors but is likely to exist.

Table 2.1: Approximate sediment budget per section between 2015 riverbed topography and 2014 corrected channel bed. Total sediment budget is calculated based on interpolated data for the 20 m upglacier of surveyed channel. Results show substantial variations between sections, with a tendency for deposition between both measured beds.

	Sedimentary budget per section (m^3)
Section n°1	-0.19
Section n°2	-1.18
Section n°3	4.1
Section n°4	-0.72
Section n°5	1.08
Section n°6	-0.90
Section n°7	7.49
Section n°8	8.03
Section n°9	-0.11
Section n°10	7.48

After establishing probable channel geometry, closure rates estimations (after Hooke, 1984) were performed (Table 2.2). For example using a 6.2 m channel radius obtained from the combination of its width and height as the observed channel is rather broad than semi-circular and ice thickness of 6.35 m, calculated creep closure after 8 months is negligible (0.0046 m) and even after 12 months it is still less than a centimetre (0.0068 m). However the Hooke (1984) calculation applies to semi-circular shapes, and since the channel is broad and low, chances are that creep closure will be slightly greater. Nevertheless, given the shallow overlaying ice, creep closure is still thought not to be the dominant process controlling the channel shape.

Table 2.2 : Channel closure calculations using the Hooke (1984) formula. Under shallow ice, creep closure is negligible even after 12 months.

	Channel radius (m)	**Ice thickness (m)**	**Closure after 8 months (m)**	**Closure after 12 months (m)**
Calculation 1	10.81	3.66	0.0015	0.0023
Calculation 2	8.53	4.88	0.0028	0.0043
Calculation 3	6.20	6.35	0.0046	0.0068

2.3.3 Discussion

GPR observations at the Haut Glacier d'Arolla seem to agree with other field reports (e.g. Hooke, 1988; Hooke et al., 1990) that certainly close to the glacier's snout, the subglacial channel shape is broader and flatter than traditionally assumed (e.g. Röthlisberger, 1972). Furthermore, surveying progressively up-glacier revealed a rapid change in the channel shape, as it became flatter in relation with overlaying ice thickness. The channel bed also evolved rapidly between sections, creating possible low flow speeds areas that might lead to deposition (shown by Table 2.1) and higher flow speed areas prone to incision (Table 2.1). Collapse on the last survey day provided visual access to the channel and revealed it wasn't full of water even during the mid-afternoon when melting was at its peak, and that water flow was concentrated at the centre of the channel on a till bed. Interestingly Röthlisberger recognized that channels near the terminus would not be full of water but never discussed the extent of open-channel flow (Walder, 2010). Theoretical predictions made by Lliboutry (1983) and Hooke (1984) showed that open-channel flow could be possible below thin ice and even under 200-300 m of ice, though field observations have never confirmed such predictions (Walder, 2010).

Using Hooke's (1984) equation and assuming semi-circular channels, Nienow et al. (1998) suggested that channels in the lower 700 m of the Haut Glacier d'Arolla would survive winter by becoming flatter due to the shallow ice thickness (~90 meters). The closure rates would be minimal to non-existent in the lowermost 500 m where ice thickness is less than 50 m (Nienow et al., 1998), suggesting that channels could survive for several years. However the authors recognized that the Hooke (1984) model applies to semi-circular channels, broad and low channel creep closure would be underestimated and it is conceivable that only near-snout channels would survive a winter (Nienow et al., 1998). Our calculations may also be underestimating creep closure, especially since our data suggest the channel is rather broad and low and

becomes quickly lower upglacier. More data collection following the channel higher upglacier would contribute greatly to answering this question.

Ground-penetrating radar surveying also revealed the existence of a radar scattering layer. Such layers are generally thought to be indicative of water containing temperate ice. Conversely, ice without radar scattering is thought to be cold under the assumption that cold ice does not contain scattering water bodies. However studies have shown that the water distribution does not always reflect the ice thermal state, hence the boundary between scattering and non-scattering layer does not always indicate the limit between temperate and cold ice (Brown, Harper and Bradford, 2009).

Potential explanations for the presence of this radar transparent layer may include the possibility of ice-cold patches resulting from winter cold waves that would not have been removed by ablation (Cuffey and Paterson, 2010). Several authors have also shown this boundary could represent the glacier hydrological system piezometric surface (Bamber, 1987; Jania et al., 2005; Jania et al., 1996). Brown, Harper and Bradford (2009) noticed the transparent layer at Bench Glacier, Alaska contains a lower density of air filled scatterers such as open fractures, thus suggesting transparent layer has limited space available for water. The question however remains whether the absence of voids is the result of the absence of water, or water is absent because there is no space for it (Brown, Harper and Bradford, 2009).

Matching the observed radar transparent layer extent in the first 5 to 10 m, borehole video observation by Copland et al. (1997) on the Haut Glacier d'Arolla revealed two rapidly changing ice type zones based on changes in air-bubble content (0 to 2 m and 5 to 20 m). The authors also reported borehole refreezing between 5 to 20 m below the glacier surface, the first 0 to 2 m only occasionally refreezing. This leads to the hypothesis of winter cold waves driven process cooling the first 20 m of ice below freezing point during winter. Warmer air temperature and solar radiation inputs on the glacier surface during melt season progressively reduce the extent of the cold layer starting from the surface and going downwards. Surface cold zone (0-2 m) results from shorter term cooling such as overnight freezing. Observations by Copland et al. (1997) appear to fit with the extent of the transparent radar layer detected during the 2014 and 2015 summers and suggest the cold wave driven layer is still present on the Haut Glacier d'Arolla to a slightly lower extent, the transition being observed at 10 m instead of 20 m.

Section II: Flow and sediment transport analysis

2.4.1 Methodology

Ground-penetrating radar estimated channel geometry suggested the formation of relatively large channels, but with flow at atmospheric pressure given possible water surface reflections (Fig. 2.2b), and substantial up glacier changes in channel geometry, with potentially important implications for sediment transport capacity. Indeed, there was the suggestion of substantial erosion/deposition during the snout retreat within these channel zones (Table 2.1).

To evaluate the processes responsible for the channel formation, western channel discharge was calculated using Shreve potential (1972) (Equation 2.2) maps and flow routing maps (Fig. 2.8). Maps were then used to split measured 2014 discharge by Grande Dixence S.A. into western and eastern channel contributions (Equation 2.3).

A flow and sediment transport capacity model (Equations 2.4 to 2.6) was then applied using sections geometry in order to evaluate the discharge to flow depth and transport capacity relation for each section and increasing flow depths (Table 2.3). Results were then compared with calculated 2014 discharge (Fig. 2.9).

2.4.1.1 Flow routing

Three shreve (1972) hydraulic potential maps – one for each value of c – (Equation 2.2) were constructed by combining Sharp et al. (1993) bed topography map with most recent (2012) high resolution DEM of the Haut Glacier d'Arolla surface (SwissAlti3D).

$$\boldsymbol{\Phi = \rho_w\, g\, z + c\,[\rho_i\, g\,(H - z)]}$$

Equation 2.2: Adapted Shreve (1972) hydraulic potential from Willis et al. (2009)

Where ρ_w is the water density (1000 kg m^{-3}), ρ_i is the ice density (910 kg m^{-3}), g is the gravity acceleration (9.81 m s^{-2}), H and z are the surface elevation and the bed elevation respectively (m). Constant c is equal to 0, 0.5 or 1 where $\rho_w = \rho_{atmospheric}$, $\rho_w = 0.5 * \rho_i$ or $\rho_w = \rho_i$.

Subsequently, three flow routing maps were constructed based on the three hydraulic potential maps, using the following method: each cell contributes its weight to all surrounding cells with lower hydraulic potentials or elevations. Transferred weight proportions are calculated using magnitude differences between the hydraulic potential or elevation gradient of the "source" and "sink" cells (Sharp et al., 1993). The flow accumulation algorithm was applied and appropriate map was chosen (Fig. 2.8). Then two sectional accumulated flow values were extracted at the glacier snout for each channel (western: A_2 and eastern: A_1) and Equation 2.3 provided discharge values for the western channel (Q2) based on total discharge measured by Grande Dixence S.A (Q_{tot}). Based on field observations, the tributaries inflows are negligible (less than 1% of the total discharge), the Haut Glacier d'Arolla is assumed to deliver almost 100% of the water.

$$Q_2 = \frac{A_2}{A_1 + A_2} * Q_{tot}$$

Equation 2.3 : Discharge splitting using sectional accumulated flow values for western and eastern channels (A2 and A1 respectively) and total discharge measured by Grande Dixence S.A.

2.4.1.2 Flow and sediment transport modelling

Flow and transport modelling was performed using a model that calculates the discharge needed to progressively fill a channel up to a flow depth of 3 m (with steps of 0.01 m). The model follows the approach of Nitsche et al. (2011), which attempts to deal with over-prediction of bedload flux that many bedload transport equations tend to do by under-estimating energy losses from bed roughness (Lane et al., in press). This approach has been widely tested in Swiss catchments (Nitsche et al., 2011; Lane et al., in press) and follows Rickenmann and Recking (2011) in treating energy loss caused by spatial organisation of bed roughness.

First, flow resistance is calculated following Ferguson (2007) velocity power equation to estimate cross-section average flow velocity (v_{tot}) (Equation 2.4). This approach allows for changing flow depth and flow resistance effects to be modelled in a reasonable way (Lane et al., in press), where R is the hydraulic radius (m), S is the slope, D_{84} is the 84th percentile of grain-size (m) and g is gravity (m s^{-2}).

$$v_{tot} = \frac{6.5(gRS)^{0.5}\ 2.5(\frac{R}{D_{84}})}{[6.5^2 + 2.5^2(\frac{R}{D_{84}})^{1.67}]^{0.5}}$$

Equation 2.4 : Ferguson (2007) velocity power equation to estimate cross-section average flow velocity

Subsequently, volumetric sediment transport capacity estimation was achieved following Nitsche et al. (2011) to calculate grain-scale velocity (v_0) without energy loss (Equation 2.5).

$$v_0 = 6.5(gRS)^{0.5}(\frac{R}{D_{84}})^{0.167}$$

Equation 2.5 : grain-scale velocity without energy loss

Then partitioning slope (S) energy line after Rickenmann and Recking (2011) into lost energy from flow resistance and energy available for sediment transport (S_0) (Equation 2.6). Estimated per unit channel width volumetric transport rate (q_b) is then given by (Equation 2.7) (Rickenmann, 1991; Lane et al., in press).

$$S_0 = S(\frac{v_{tot}}{v_0})^{1.5}$$

Equation 2.6 : Partitioning of slope energy into lost energy and energy available for transport

$$q_b = (\frac{\rho_s}{\rho g {D_{50}}^3})^{0.5} 2.5\sqrt{\theta_r(\theta_r - \theta_{rc})Fr}$$

Equation 2.7 : Estimation of volumetric sediment transport rate per unit channel width, where ρ is the water density, ρ_s is the sediment density (2650 kgm^{-3}), θ is the shear stress reduce with Equation 2.4 and θ_{rc} the reduced critical shear stress. Fr is the Froude number defined by $v_{tot}/(gd)^{0.5}$ d being the mean flow depth.

Discharge and sediment transport capacity models were run using the 2014 GPR data channel roof and the channel bed after correction for air-layer induced wave speeds acceleration. As uncertainties are important regarding the corrected bed reliability, calculations were repeated using the 2015 riverbed extracted from photogrammetry scan for results comparison. It has been shown previously (see 2.3.2 Results, Fig. 2.6 and Table 2.1) that 2014 channel bed conditions are different to 2015 bed conditions notably due to erosion and deposition processes.

Grain-size samples were taken at western subglacial channel exit in 2015 (D50=0.016, D84=0.067) (P. Perolo, personal communication, August, 2015) but are possibly not representative of the grain in the channel at the time of the ground-penetrating measurements. It is likely that grain-size values are fluctuating through time as streams are known for sorting sediment on both space and time scales. To evaluate the effects of such variability, four sets of grain-size values were tested for each calculation (Table 2.3, p. 41).

2.4.2 Results

2.4.2.1 Flow routing and discharge separation

Resulting Shreve potential and flow routing maps (Fig. 2.8) demonstrate the existence of a major drainage axis on the glacier centre line, drainage pattern varies however depending on the water pressure. At atmospheric pressure only one major channel seems to exist, with $\rho_w = 0.5 * \rho_i$ water is more widespread on the bed and a second drainage axis appears on the western side fed by the western side of the glacier inflow. Map 2.8c clearly shows two main subglacial drainage axis, one on the glacier centre emerging on the glacier eastern snout side, the other following closely and emerging on the western side of the glacier. This reconstruction is thought to follow field observations and was thus used for discharge partition, even though conflicting with Hooke (1984) predictions of open channel flow under most of the Haut Glacier d'Arolla. This is a source of uncertainty in our calculations; visual field observations confirmed however that both channels appear to deliver approximately equivalent discharge, with a slight advantage to the eastern channel. The response time to melting during the day was also observed to be slightly different.

Using reconstruction C (Fig. 2.8c), western channel contribution to the mean total discharge (4.6 $m^3\ s^{-1}$), after Equation (2.3) is 46% (2.1 $m^3\ s^{-1}$) and eastern channel delivers the remaining 2.5 $m^3\ s^{-1}$. Maximum total discharge measured during summer 2014 by Grande Dixence SA was 11.5 $m^3\ s^{-1}$, which leaves 5.3 $m^3\ s^{-1}$ in the western channel and 6.2 $m^3\ s^{-1}$ in the eastern channel.

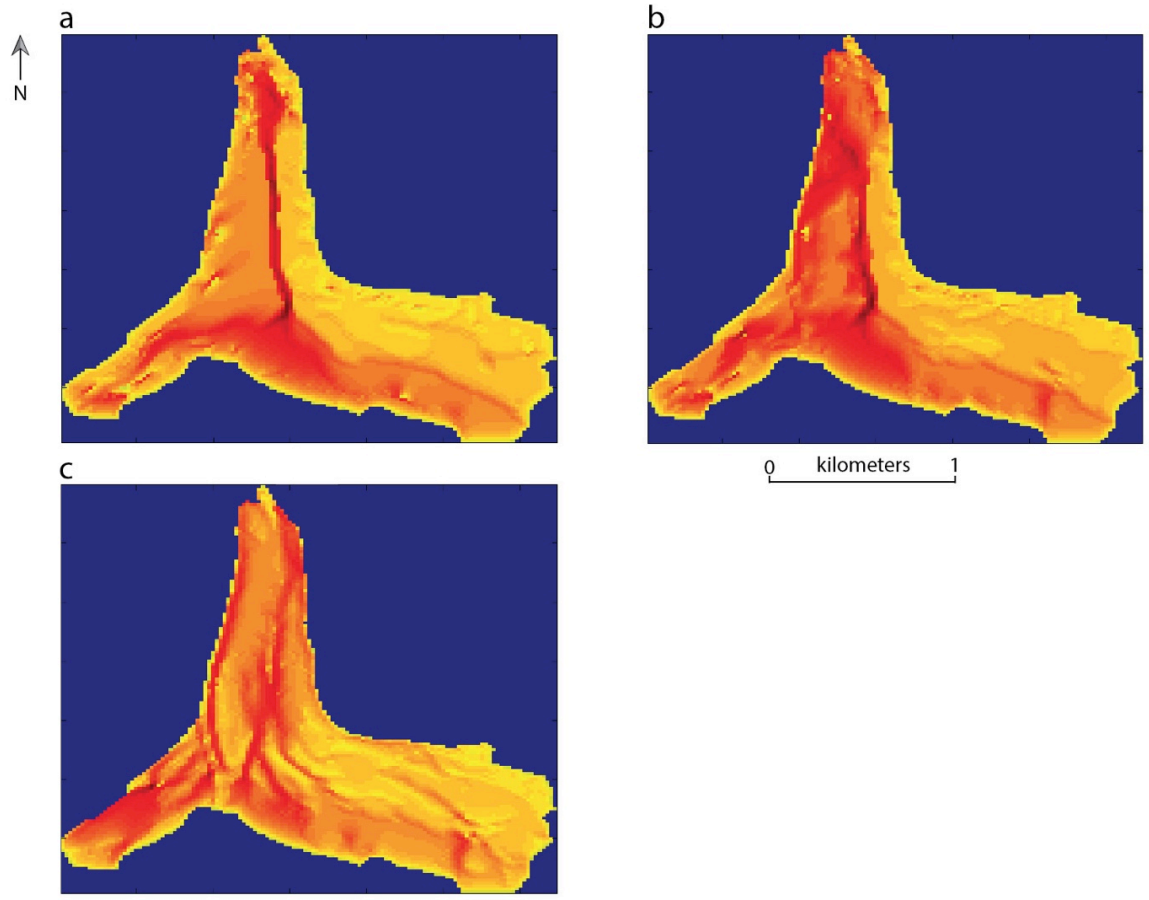

Figure 2.8 : Flow routing maps based on adapted Shreve (1972) hydraulic potential (Willis et al., 2009). Map (a) corresponds to water pressure = atmospheric pressure, map (b): water pressure = 0.5*ice overburden pressure, map (c): water pressure = ice overburden pressure. Widespread atmospheric pressure following Hooke (1984) hypothesis demonstrate the existence of one major subglacial channel following the glacier centre line. Map (b) of $p_w = 0.5*p_i$ shows extended flow near the glacier snout and the appearance of a second subglacial channel on the glacier western side. Finally (c) $p_w = p_i$ indicates a more tree-like drainage pattern, creating two major channels: one on the glacier centre line exiting on the snout's eastern side, the other closely following the western side of the glacier. Map (c) is thought to be the most similar to field observations and was used for discharge splitting.

2.4.2.2 Sediment transport capacity modelling

For both bed topography datasets, all sections and different sets of grain-size values, the model shows that low flow depths are sufficient to reach the calculated mean and maximum discharges: so that it is extremely difficult to fill the measured subglacial channel geometries with the maximum discharges typical of this glacier. For example using the GPR corrected bed topography and a section taken 9 m downglacier of the highest GPR line (section n°5 in Fig. 2.6) – this particular section was picked due to the strong similarities between both bed topography data – a water depth of 0.24 m is sufficient to reach the average 2.1 m^3 s^{-1} discharge with the smallest grain-size (Table 2.3), and fill less than 5% of the total channel area. Maximum calculated discharge (5.3 m^3 s^{-1}) would be reached with a flow depth of 0.34 m. In fact extreme discharge values would be required to fill only 50% of the channel (Table 2.3).

Comparing results from both bed topography datasets (Table 2.3), it appears that the usage of the GPR extracted bed is resulting in lower flow depths and higher transport rates for small sediments than the 2015 riverbed, the difference being however rather small, in the order of 0.10 m^3 s^{-1} or less depending on the grain-sizes values. The same observation can be made for the flow depths. It appears however that the 2015 riverbed has more capacity to transport large sediments during storm events.

The discharges required to fill the channel to 50% are, however, different between the datasets to a significantly higher order of magnitude. Given that the maximum 2014 discharge measured by Grande Dixence S.A. was 11.85 m^3 s^{-1} for both channels, the discharge values required to fill the channel cannot be reached, demonstrating that the channel under the survey area was only partially filled and at atmospheric pressure during the survey.

Another important observation about Table 2.3 is that as grain-size increases, flow speed decreases due to rising drag and flow tortuosity effects, reducing flow erosion and transport capacity, but raising flow depth. This effect is shown in Table 2.3 as transport rate rapidly decreases to zero while flow depth rises.

Table 2.3 : Table of bedload transport rate and flow depth for sample section (n°5, Fig. 2.6) taken 9 m downglacier of the highest GPR survey line. The table summarizes the modelled values obtained using four sets of grain-size values and two different bed topographies, for an average discharge of 2.1 m^3 s^{-1} and a maximum discharge of 5.4 m^3 s^{-1}. Results demonstrate lower flow depth using corrected GPR bed and substantially more transport for the smaller grain-sizes values: the mean discharge is attained with a water depth of 0.24 m and 0.35 m for maximum discharge instead of 0.31 and 0.43 respectively. In both cases transport rate rapidly decreases to zero as grain-size values and flow depth increase. The last column shows the modelled discharge values required to fill 50% of the channel with water, revealing unreachable discharge values in both cases. Calculated transport values also assume sufficient sediment supply to transport sediment at the capacity suggested by the equations.

	Discharge (Q) = 2.1 m^3/s		*Discharge (Q) = 5.4 m^3/s*		
Section n°5, corrected GPR bed	**Flow depth (m)**	**Transport (m^3/s)**	**Flow depth (m)**	**Transport (m^3/s)**	**Discharge to fill channel to 50% (m^3/s)**
D50=0.016 m D84=0.067 m	0.24	0.104	0.35	0.351	290
D50=0.05 m D84=0.08 m	0.25	0.048	0.36	0.22	280
D50=0.1 m D84=0.16 m	0.31	0	0.43	0.01	225
D50=0.2 m D84=0.32 m	0.38	0	0.53	0	160
Section n°5, riverbed DEM	**Flow depth (m)**	**Transport (m^3/s)**	**Flow depth (m)**	**Transport (m^3/s)**	**Discharge to fill channel to 50% (m^3/s)**
D50=0.016 m D84=0.067 m	0.31	0.08	0.43	0.3	245
D50=0.05 m D84=0.08 m	0.32	0.036	0.45	0.22	235
D50=0.1 m D84=0.16 m	0.38	0	0.53	0.05	180
D50=0.2 m D84=0.32 m	0.47	0	0.65	0	130

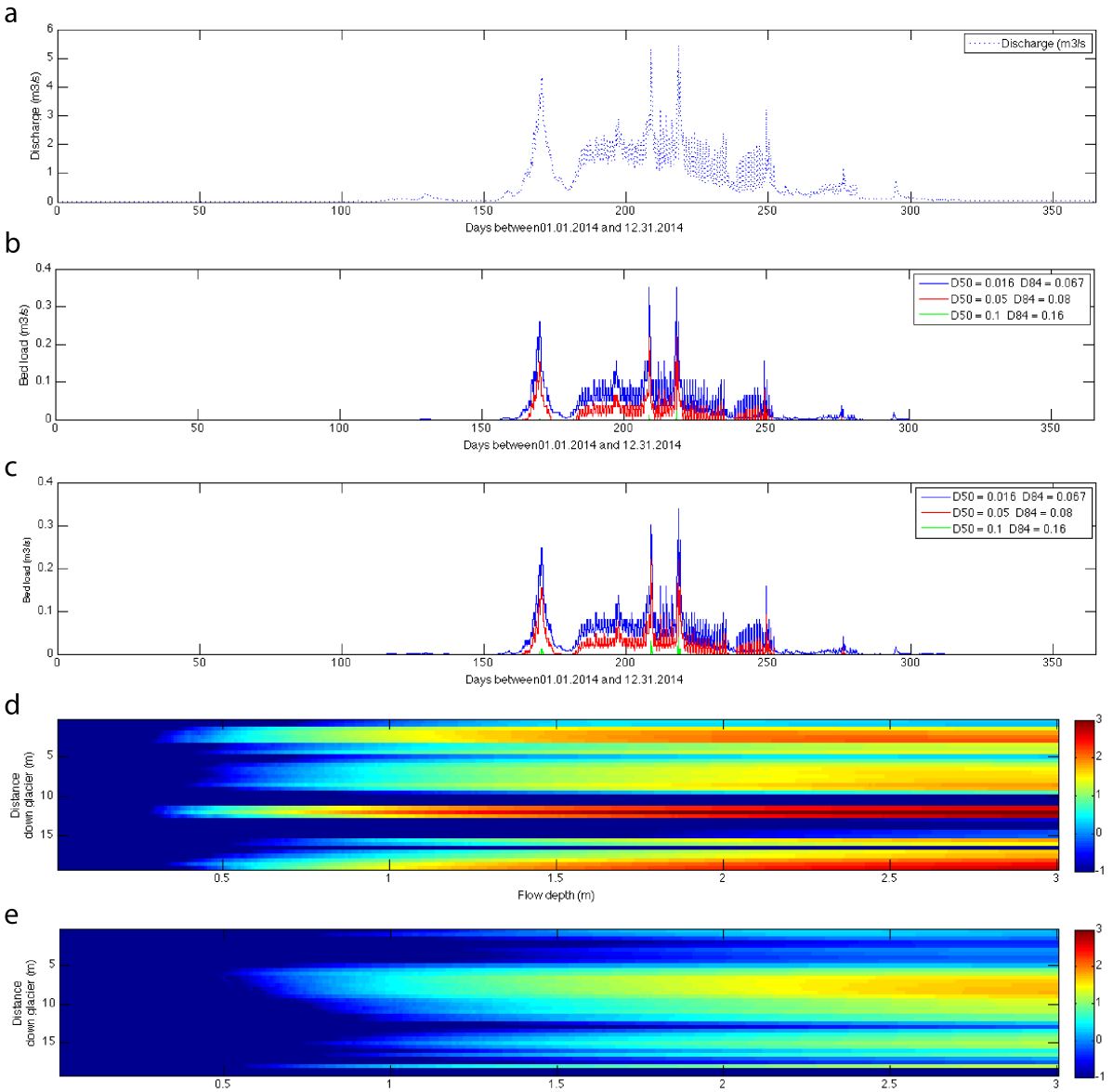

Figure 2.9 : (a) Discharge values measured every 15 minutes from 01.01.2014 to 12.31.2014 and reduced to correspond to western channel contribution. Discharge demonstrates monthly scale variations (melt season), weather related variations (storm events) on the inter-daily scale and intra-daily variations due to afternoon melting events (diurnal cycles). (b) Related modelled bedload transport values for 2014 GPR extracted and corrected channel bed, using four sets of grain-sizes values. (c) Shows the modelled bedload transport for the 2015 riverbed extracted bed and same sets of grain-sizes values. (b) and (c) demonstrate similar substantial transport rate for smaller grain-size with low critical discharge closely following the discharge peaks: bedload transport is higher during afternoon peak discharge and during storm events. Increasing grain-size values dramatically reduce transport to storm events only, and to no transport at all for the last set of grain-values (constant zero values not presented on the figures). (d) Spatial distribution of volumetric bedload transport rate in relation with flow depth and for a given set of grain-size (D50=0.1, D84=0.16) and the 2014 GPR extracted channel bed topography, (e) shows the results for the 2015 extracted riverbed topography. (d) and (e) reveal substantial downglacier variations in bedload transport, however (d) shows variations to a significantly higher magnitude. Fluctuating transport rate between sections is thought to lead to successive sediment deposition and erosion, possibly sediment clogging and flushing events.

Critical discharge and its relation to grain-size are key elements driving bedload transport rate as shown by the peak discharge-transport relation between Fig. 2.9a, 2.9b and 2.9c. The 2014 discharge (Fig. 2.9a) demonstrates high variability in glacier melting process and meltwater output on a monthly scale as well as inter-day to intra-day scales. Melt season, weather conditions and diurnal melting cycles can be seen as the main sources of discharge variability, which translates into bedload transport rate variability as revealed in Fig. 2.9b and 2.9c: transport process does not happen continuously but is tightly linked to the discharge rate on all scales. Storm events marked by dramatic discharge increase, strongly impact transport rate. On a different time-scale, melting marked by daily oscillations (Fig. 2.9a) increases discharge hence transport (2.9b, 2.9c). Furthermore the smallest grain-size (D50=0.01, D84=0.016) set in our calculation shows substantial transport rates (Fig. 2.9b, 2.9c), the third set however (D50=0.1, D84=0.16) demonstrates transport only happening during storm events. Larger grain-sizes suggest that no transport occurs with measured discharge in the western channel. Figures 2.9b and 2.9c show close similarities in transport rate response to discharge variations, with slightly greater transport capacities in 2.9b (GPR corrected bed) than in 2.9c (2015 riverbed).
Figure 2.9d and 2.9e show substantial downglacier variations in bedload transport due to significant changes in bed topography and inter-section slopes suggesting important erosion and deposition fluctuations between sections, possibly leading to clogging and flushing events. Corrected GPR bed (2.9d) indicates stronger downglacier variations, signifying possible clogging and flushing events to an even larger order of magnitude.

2.4.3 Discussion

Flow routing maps showed the existence of a major subglacial drainage channel on the glacier centre line for all three water pressures. The western channel seemed only to exist using a water pressure equivalent to ice overburden pressure, which conflicts with Hooke's (1984) prediction of open channel flow on most of the Haut Glacier d'Arolla as well as borehole observations by Hubbard et al. (1995) where water pressure ranged from atmospheric to exceeding ice overburden. As noted by Gulley et al. (2012a), Shreve (1972) hydraulic potential calculation is based on a number of assumptions regarding glacier internal properties that are most likely never met, such as uniform water pressure under the glacier, identical rates of conduit enlargement and creep closure at every point of the glacier, uniform water inputs, and homogeneous isotopical permeability distribution. Incorrect assumptions may explain the discrepancies between the observed subglacial drainage system and its modelled counterpart. Uniform recharge assumption is possibly one of the most problematic as water inputs from basal melting (1-100 mm a^{-1}) is of a very different magnitude from punctual inputs by moulins (1000-10000 mm a^{-1}) (Gulley et al., 2012a), which in turn could have a major impact on subglacial water pressure distribution. This emphasizes the need for a more complex model to determine the drainage axis inside glaciers based on discrete recharge effects by moulins, varying water pressures and fluctuating conduit enlargement and creep closure, such as the physically based model of glacier hydrology created by Arnold et al. (1998). Consequently the current discharge splitting using hydraulic potential should be taken with care, even though field observations showed approximately equal contribution from both streams. Another possible explanation of the discrepancies between the Shreve model predictions and the field observations would be the existence of legacy channels. This hypothesis is discussed further below.

Flow modelling using two datasets of bed topography showed similar response to increasing grain-size with slightly lower flow depth and more transport with the 2014 bed topography. This seems to indicate that the bed correction applied to the GPR dataset is mostly reliable, it is however an open question whether the significant topography variations resulting in strong transport rate differences in Fig. 2.9d can either be the result of GPR-induced errors, or are demonstrating real changes between sections.
Modelling revealed the channel sections could not be full of water and even 50% water filling could not be reached with measured discharge. Moreover, sediment transport capacity modelling showed important variability in transport on both time and space scales; substantial transport variations between sections coupled with monthly to daily scale discharge magnitude change may lead to erosion and deposition episodes fluctuating in time between sections and possibly leading to sediment clogging of certain areas with time. Additionally modelled bedload transport rates are particularly low due to low hydraulic radius and wide channel dimension, allowing water to spread out and loose most of its energy. Processes translate into a sediment-sorting phenomenon as fine sediments are transported, while larger ones remain. Supporting these observations, high grain-size values in the model demonstrated no bedload transport. On the contrary using grain-size values close to the ones determined in the field in 2015 at the glacier snout, demonstrated substantial transport rate.
Reports of largely fine-sediment depleted conduits have been made on other glaciers (e.g. Gulley et al., 2012a) suggesting the hypothesis that smaller sediments may have been washed away throughout the melt season, creating downward incision in the till and leaving larger sediments and boulders (>1m) behind. Once discharge decreases below critical level at the end of the melt season, small sediments would likely start depositing, especially in low flow velocity areas, leading to clogging areas behind boulders, which would act as sediment trappers. This leads to the possible supposition that peak channel size was reached when 2014 ground-penetrating radar survey was undertaken at the peak of melt season, and sediment deposition was already happening when 2015 photogrammetry scans were performed, thus explaining substantial deposition phenomenon showed by Table 2.1.

The hypothesis of a sediment driven process can be proposed to explain observed channel geometry (Fig. 2.11, p. 48), and this hypothesis is thought to be valid on various time-scales: year-to-year scale, seasonal-scale and daily scale depending on channel dimensions and sediment supply. Step 1 (Fig 2.11, p. 48) assumes minimal discharge conditions with negligible to null sediment transport (winter period or during the night). Assuming maintained supply, sediments would have accumulated and filled the channel. (2) With increasing discharge (for example caused by the beginning of melt season or by the diurnal melting cycle), pressure would start to build up in clogged channel as hydraulic radius would be too small to accommodate for sudden discharge increase (Gulley et al., 2013). This would result in raising the glacier and increasing ice-flow speed (Hubbard et al., 1995) such as possible hydraulic jacking observed by Gabbud et al. (2015) in the near snout area of the Haut Glacier d'Arolla. Trapped fine sediments would then be flushed, enlarging the channel downward, sideways by bank erosion and upward by ice ceiling melting. As a consequence, subglacial channel pressure would drop back to atmospheric and glacier would slow down. Bank erosion could destabilize the overlaying channel ceiling resulting in small collapses, enlarging the channel further (3). Creep closure is thought to be almost non-existent under shallow ice conditions such as observed in our survey location (Hooke, 1984), allowing

for channel to grow to large extents. Progressive fine sediment flushing, may lead to situations where only large boulders would remain on the riverbed (Gulley et al., 2013), increasing flow tortuosity and encouraging sediment deposition and clogging as discharge decreases (4a, 4b), which would then lead to situations such as (5b) and then back to (1 and 2). This sediment driven process may also happen on the year-to-year timescale, depending on sediment supply quantity and discharge variations; for example between warm and cold years, or when the glacier is in a severe retreat period while the channel remains in place and does not close (non-existent creep closure). This would result in discrepancies between channel size and actual discharge leading the hypothesis of possible legacy channels: These channels would have been created under previous substantial discharge and sediment supply conditions, causing the channel to enlarge significantly into overhead ice ceiling and sediment bed. These channels would have remained in place, not closing due to thinning of overhead ice thickness and diminishing sediment supply as the glacier retreats. This could be one explanation of why the Shreve (1972) model predictions seemed to only agree with field observation using water pressure equal to ice overburden; indeed channels on the Haut Glacier d'Arolla may very well have formed under very different water pressure conditions, and have stayed in place since then. In fact, Sharp et al. (1993) determined using dye-tracing that channels seemed to reform annually along preferential drainage axes on the Haut Glacier d'Arolla. The channels may actually stay opened under reduced form and high flow tortuosity due to low flow depth could have created BTCs that would have looked like ones from a distributed system, as suggested by Gulley et al. (2012b).

Furthermore and supporting the proposed channel evolution hypothesis (Fig. 2.11), studies have demonstrated high sediment availability at the beginning of the melt season due to accumulated sediments throughout winter on various glaciers (Liestøl, 1967; Hooke et al., 1985; Collins, 1989) and sediment flushing with the first discharge increase (Swift et al., 2005a), leading to spring events and increased basal sliding (Collins, 1989; Hooke et al., 1985), followed by a reduction of sediment availability, which has been interpreted as a sign of general sediment exhaustion (Hooke et al., 1985) or the sudden limitation of water flow to newly formed subglacial channels where exhaustion happens rapidly (Collins, 1989). Following the proposed model, it is indeed likely that reduced sediment availability is due to exhaustion in the channel. It is also possible that the spring events are not simply related to distributed to conduit subglacial drainage transitions, but also the effects of accumulated sediment on preventing efficient flow drainage.

In near-snout situations and thin overlaying ice conditions, melting from the surface contributes to thinning the ice layer, eventually resulting in a channel roof collapse (4b) as was observed on the western channel. With glacier retreat, the subglacial channel would progressively become part of the sandur area (5a).

Remains of an unroofed subglacial channel on the eastern side of the glacier snout are evidence of similar processes happening regularly in the glacier near-snout area (Fig. 2.10). The channel is however narrower than the observed western one, suggesting roof collapse was only caused by surface melting and not by channel widening to an unstable extent. Channel is however significantly too large to accommodate eastern channel discharge and bears significant marks of water-induced erosion on its banks and up to its roof, hinting channel to have evolved as suggested by the previously evocated hypothesis: through progressive downward incision by sediments evacuation. A similar collapse process was also observed on a vastly larger extent on the Glacier de Ferpècle in summer 2015 when 400 m by 200 m area collapsed in the glacier snout over a possible subglacial channel.

Figure 2.10 : Relics of a subglacial channel in dead-ice located on the eastern part of the Haut Glacier d'Arolla. Instead of channel closure due to overlaying ice weight, near-snout channel roof supposedly collapsed as a result of glacier surface melting. Here the channel ice walls bear the traces of erosion by water and turbulent flow suggesting mutual processes of channel enlargement through ice wall melting and bed erosion. Channel bed is composed of till ranging from fine sediments to large boulders (Personal picture, August 2014).

Similar to the eastern channel relics (Fig. 2.10), our channel also appeared to change shape rapidly in width and height but less sinuous. Rapid changing subglacial channel shape was also noticeable in recent subglacial channels mapped by Gulley et al. (2012a) who pointed out that channels were generally broad, low and locally anastomostic. Speleological exploration of the drainage system revealed that channel shapes changed constantly and were never the straight semi-circular shape as predicted by theory. Mapping was however performed on a cold base glacier. Processes are likely to be different on a warm based glacier.

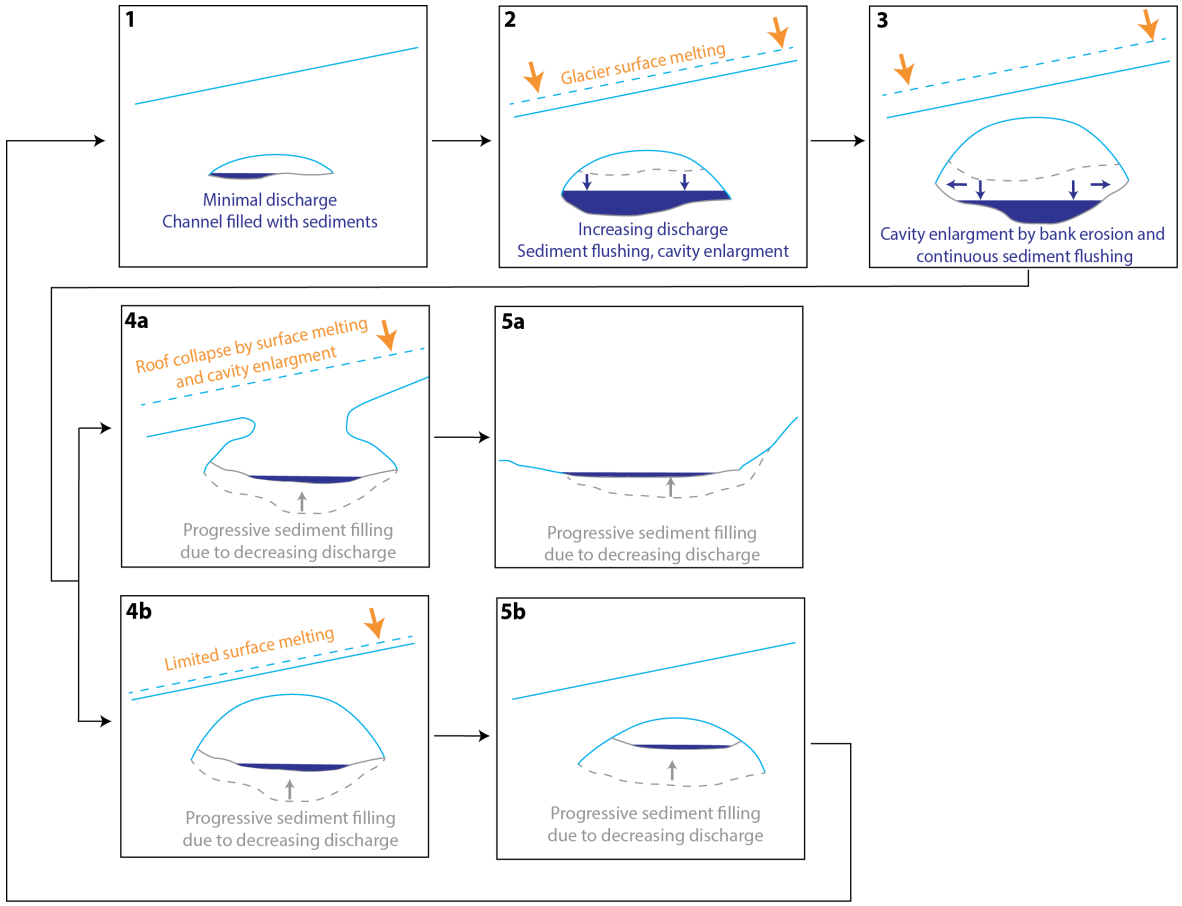

Figure 2.11 : Near-snout subglacial channel evolution hypothesis based on field observations and data analysis: (1) During minimal discharge periods (winter or night for example), transport of glacier-eroded material is negligible and channel bed would rise by sediments accumulation. (2) With increasing discharge (beginning of melt season, diurnal melt cycle), trapped sediments would be evacuated, enlarging the channel bed downward and sideways (3). Under thin overlaying ice conditions, creep closure is thought to be negligible, allowing for wide cavity development. However surface melting may provoke channel roof collapse by progressive thinning of the overlaying ice (4a and 5a). With decreasing discharge the channel bed would progressively get filled with sediments (4a, 5a, 4b, 5b) until the following discharge increase starts the cycle again (2).

2.6 Conclusions

Ground penetrating radar profiles near the snout of the Haut Glacier d'Arolla have allowed insight into a major subglacial channel. The channel was followed for 20 m, and evidence suggested the channel to be significantly larger than expected, evolving from 21 m to 13 m width and from 3 m to 1.6 m in term of channel height as the ice thickens. Channel roof collapse provided visual confirmation of the ground penetrating radar measurements.

Using the extracted channel geometry from the GPR data, discharge modelling demonstrated the flow depth to be significantly lower than expected, the channel never being full of water based on discharge records for the Haut Glacier d'Arolla, thus confirming other reports of near-snout atmospheric channel flow (e.g. Hooke, 1984).

Available evidence suggests a combination of channel bed erosion by successive sediment flushing, absence of creep closure and surface melting processes to creating wide near-snout subglacial channels. More observations are needed to verify whether this mechanism is truly dominant in the production of near-snout channels, or specific to some glaciers. In fact, the dynamics of subglacial channels may be due as much to the development of progressively more efficient drainage networks through sediment transport as it is due to ice melt, suggesting new research possibilities by studying subglacial river bed conditions and sediment driven mechanics in ice-carved subglacial rivers where ice dynamics are dominant, versus till-carved subglacial rivers where till dynamics are prevailing.

Finally, evidence of a winter cold wave driven layer was provided by the presence of a radar transparent layer in the first 10 m of ice on the glacier-wide profiles. Near surface borehole refreezing was reported on the Haut Glacier d'Arolla by Copland et al. (1997), corroborating the cold wave driven layer hypothesis.

Part III - Conclusions

Chapter picture
Air Glacier « Lama » helicopter taking off the Haut Glacier d'Arolla (top picture, 07.30.14)

Mont Brulé and accumulation area of the Haut Glacier d'Arolla (bottom picture, 08.04.14)

3.1 Methodological potential

This study demonstrated the relevance of using ground-penetrating radar techniques in subglacial research, notably its ability to highlight glacier bed conditions, subglacial channel position and intra-ice conditions in the near-snout area. Provided certain conditions are met, such as low water content in the ice and low scattering amount, accurate data can be acquired and subsequent data processing may provide high quality feature reconstruction.

The potential of drone photogrammetry to provide centimetre-scale data over glaciated terrain, sediment covered terrain and streams, was also demonstrated. Subsequent construction of high-density point clouds, meshes and orthophotos makes it a highly valuable method for low-cost short-term repeated measurements (Fig. 3.1).

The combination of intra-glacial and subglacial data acquired using ground-penetrating radar techniques with surficial data obtained using drone photogrammetry can provide valuable data on subglacial channel geometry and its potential evolution over the course of a melt season.

Figure 3.1 : High resolution hillshaded digital elevation model obtained using drone photogrammetry, revealing extremely detailed features both on the Haut Glacier d'Arolla and in the proglacial area.

3.2 Limits and perspectives

A number of technical limits must however be pointed out regarding the applied methods. Ground-penetrating radar is an indirect method, which means it provides information on the subsurface structures but it is however not sufficient to solely draw absolute conclusions with. Thus direct measurements such as boreholes or in this case, visual access to the channel, are necessary to validate the assumptions on the subsurface structures. Furthermore ground-penetrating radar data processing may bring to light hidden features or rectify reflectors positioning, but significant image errors are possible as processing depends on a number of possibly wrong assumptions made on the subsurface conditions.

Ground-penetrating radar is very sensitive to electrical conductivity and dielectrical permittivity contrasts between materials and a portion of energy will be lost on every encounter. As a result, radar waves will be less scattered and able to go much deeper in low water containing glaciers such as polythermal and cold glaciers, producing stronger reflections at greater depth. To ensure good quality results, glaciers should not be wet snow covered, or covered by surficial meltwater streams, nor containing too many englacial streams. High-resolution ground-penetrating radar surveys should be repeated on other glacier snouts to confirm its ability in assessing subglacial channel geometry at shallow ice depths. GPR survey areas should also be extended to thicker ice zones in order to evaluate capability to follow channels over greater extents and at greater depths, and a new generation of GPRs should facilitate the work notably due to their much better portability and data acquisition capabilities such as high trace stacking to greatly improve the signal to noise ratio. Additionally, 3D ground-penetrating radar data acquisition would be of considerable benefit exploring intra-glacial and subglacial features.

Evaluating near-snout channel geometry on different glaciers would allow assessment of the correctness of proposed channel evolution theory in near-snout conditions, evaluate the legacy channel hypothesis, and continue building knowledge on this particular subject as well as contributing to improve general subglacial channel theories and sediment transport under glaciers. We suggest the combination of high-resolution methods in order to evaluate the hypotheses under multiple axis of research. First off, by establishing subglacial channels positions and a DEM of the glacier bed using ground-penetrating radar. Then performing surficial drone photogrammetry scans to acquire surface DEMs and orthoimagery. Combination of methods could allow the Shreve (1972) model to be tested and compared with detected channel position; additionally the surface DEM could allow establishing glacier-surface drainage axis in combination with high-resolution orthoimage to locate active moulins position, thus the main recharge (inputs) points for the subglacial system. This could lead to possible Shreve (1972) model adaptation to take into account non-uniform recharge, as well as evaluation of the theory stating that channels generally start at the bottom of moulins (Gulley et al., 2012a). Secondly, dye-tracer injections should be performed early in the melt season in moulins and also in boreholes far from subglacial channels in order to compare BTCs of distributed system and that of the probable channelized system, and establish whether channels may survive winter (Gulley et al., 2012b) and to what extent upglacier. Measurements should then be repeated throughout the melt season to evaluate the evolution of both channelized and distributed system, possibly contributing to understand the interactions between both morphologies. New technologies capabilities offer great opportunities to better understand yet poorly known phenomenons.

Part IV - Annex I and References

Chapter picture
Haut Glacier d'Arolla and Mont Brulé (top picture, 07.31.14)

Dent Blanche behind the Bouquetin ridge on the left, and the Dent d'Hérens on the right. The Haut Glacier d'Arolla in front of the Bouquetins ridge (bottom picture, 08.04.14)

4. Annex I

4.1 Ground-penetrating radar surveying

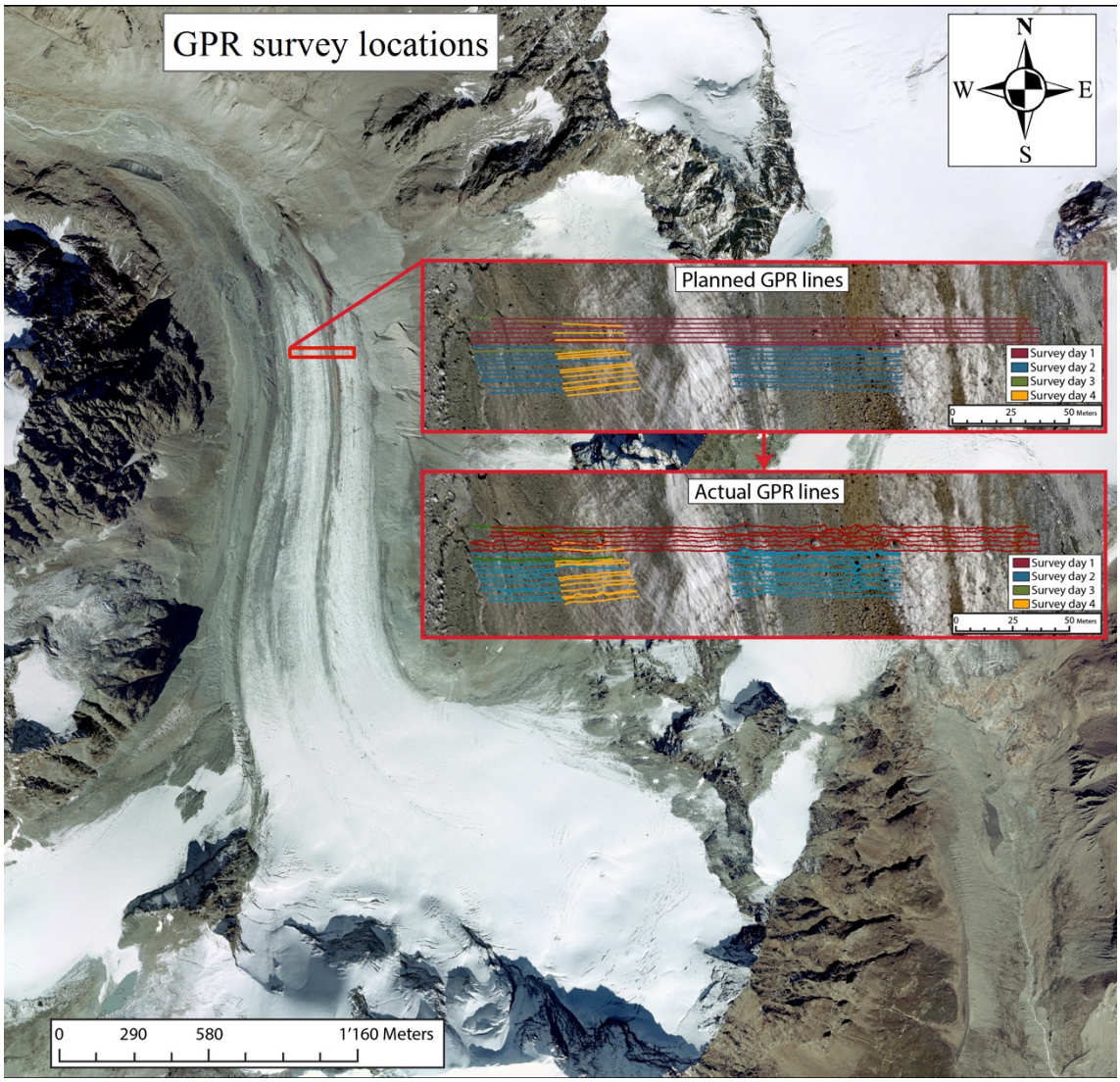

Figure 4.1: Survey location map with planned survey lines and actual GPR lines as recorded by the dGPS. SWISSIMAGE 2009 aerial orthophoto is used here, glacier has melted substantially since then and survey was located close to the snout in 2014.

Ground-penetrating radar is a relatively recent applied geophysical method, which has the potential to provide sub-meter-scale images of subsurface heterogeneity depending on frequency and ground conditions.

GPR is based on the fundamental principles of radar (Radio Detection and Ranging). Radar basically works using electromagnetic wave emissions to detect distant objects. Detection of a simple object implies that it reflects some of the energy depending on dielectric permittivity differences and electrical conductivity differences between the object and the surrounding material. The returned energy is also function of the object's geometry. The distance to the object is defined by calculating the time between signal emission and signal return multiplied by the speed of the host material, and then divided by two (the registered time expressing the back and forth time). In a uniform host material, the longer the signal takes to return, the more distant the object is (Annan, 2001).

Detecting an object also implies that it scatters energy and the scattered energy reaches the receiver antenna. The frequency used, host material conductivity and diffractions are three crucial parameters in this case (Annan, 2001):

- The more conductive a material is, the more wave attenuation there is.
- Wavelength scale heterogeneities scatter the electromagnetic waves, which implies that scattering increases with increasing frequency.
- The higher the frequency, the better the resolution. However the penetration depth is inversely linked with frequency. Therefore to see objects of various sizes at various depths, a trade-off must be found between desired resolution and workable resolution depending on the field's characteristics.

Here a pulseEkko Pro GPR system was combined with a custom built portable contraption allowing one person to carry both 100 Mhz antennas at constant offset (1 m) just above the glacier surface with a dGPS rover in the backpack, GPR console was carried by a second person. The dGPS used was a Trimble R10 GNSS/GPS/Glonass systems setup in Real-Time Kinematic (RTK) mode and with the rover directly connected to the GPR console. Trace stacking was set to 8 as a compromise between quality and number of traces collected per second.

Survey lines were performed on the east-west axis, perpendicularly to the glacier flow, with 2 m spacing between each line. 60 survey lines were performed including: (i) 7 glacier wide profiles to maximize chances of multiple channels detection; (ii) 12 profiles on the glacier's central moraine where an eastern subglacial channel was thought to be; (iii) 25 shorter profiles more focused on the western subglacial channel 20 m upglacier; and (iv) two lines repeated every 30 minutes over the course of one day above the subglacial channel (16 lines). Terrain roughness caused deviations from planned straight survey lines (as shown in Fig. 4.1.) and subsequent position correction had to be applied (see GPR coordinates smoothing (4.2.3) and binning (4.2.4) sections).

4.2 Data processing

4.2.1 Processing steps

Data were processed using MATLAB software and steps included dewow filtering, gain filter, data binning, topographic correction and noise removal through principal component analysis filtering. Plus F-K migration using codes from the Crewes Project (Margrave and Bancroft, 1996). Finally manual picking was performed to highlight specific features and allow data extraction for further analysis. The processing steps are explained below in more detail.

4.2.2 Dewow and Gain

Ground-penetrating radar data are often superimposed on low-frequency transients due to the inductive response caused by the GPR's pulse low-frequency component, thus the first step is to "dewow" the data. To this end, we used a residual median filter (Gerlitz et al., 1993) with a specified number of points for the median filter window (odd integer) of 35 in this case.

$$gain = \frac{t+1}{scaling\ factor}^{power\ to\ use}$$

Equation 4.1: Power gain equation. Parameter used were 1 for the *scaling factor* and 1.1 for *power.*

As radar signals are rapidly attenuated through propagation in the ground, signals from great depths are small. Thus displaying together shallow depth and great depth information is hard: signal from great depth is usually barely visible or even invisible. A solution is to equalize the amplitudes with a time dependent function to compensate for the rapid signal attenuation (Fig. 4.2). There are many different gain techniques; for example in stratigraphy it is important to display all the data information, thus an automatic gain control can be used (AGC, average signal is computed for each trace over a time window and the point at the centre of the window is amplified). Most importantly: applying a gain should modify the data without adding artefacts and keeping data usability (Annan, 2001).
In this particular study, the data were gained through a smooth gain function raising the time vector to a power of 1.1 (Equation 4.1).

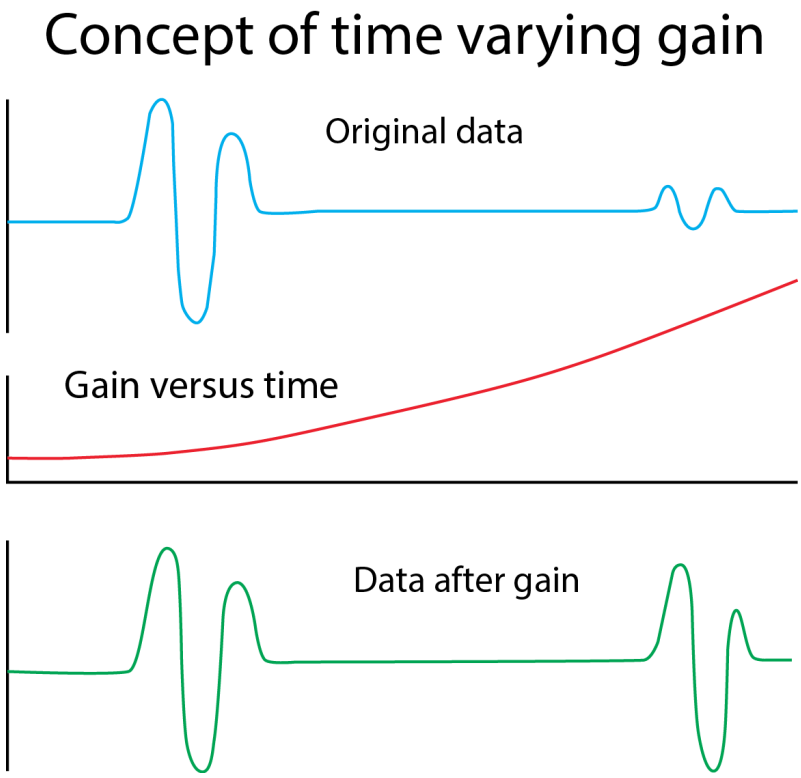

Figure 4.2: Concept of time varying gain. After Annan (2001), modified

4.2.3 GPS coordinates smoothing

Due to the glacier surface roughness, boulders to avoid and the time steps on which NMEA strings were sent from the dGPS rover to the GPR console, the position vectors had staircasing in the z axis (altitude) and spikes in the x,y axis (Fig. 4.1, actual GPR lines). Thus smoothing the vectors was a necessary step before binning the data, also improving the general visualization.
The smooth function from the MATLAB library was used to smooth out the position vectors with the 'loess' method and 20% span of the data.

4.2.4 Binning, topographic correction and stacking

Data were acquired in freerun mode but walking speed during acquisition was not constant due to glacier surface roughness. Thus the profiles had to be corrected using the dGPS position (Fig. 4.1) recorded for each trace with a technique called binning.
The idea is to group traces depending on their position into bins with a defined width (0.25 m in this case). Binning was made easier thanks to the fact that profiles were done on an East-West axis, thus grouping was only necessary on one axis otherwise data would have had to be binned relative to the survey line orientation. Following the binning process, data were then corrected for altitude using dGPS z coordinate and then stacked together in order to improve signal-to-noise ratio.

4.2.5 Principal Component Analysis filter

A reverberation effect can be seen in the first 10 to 15 m in most of the profiles (Fig. 4.3a). The unshielded RS232 cable running from the dGPS rover to the GPR console most likely caused the ringing effects. As the person holding the console could not always have the cables tightened, they were sometimes swinging near the antennas, explaining stronger reverberations at times. A recommendation for next studies using the same contraption is to use either a shielded cable or a Bluetooth connection (Bluetooth frequency is very high and won't affect GPR data) between the rover and the console.
Although the ringing is not constant across each GPR profile, it is generally easy to predict, which is not the case for the glacier GPR reflections. Thus, a Principal Component Analysis (PCA) can be used to separate predictable noise (ringing) from the signal we wish to keep (glacier reflections). The concept of a PCA analysis is to reduce the dimensionality of a matrix containing a large number of interrelated variables by extracting the dominant patterns while retaining most of the variations. The extracted dominant patterns are a new set of uncorrelated variables called principal components. Generally, the first principal components explain most of the variation in the original data set.
In this case five principal component basis vectors were extracted from the GPR data set and used to reconstruct each trace. The predictable reverberation was then removed by subtracting the reconstructed data from the real data. See (Fig. 4.3) for comparison between unfiltered data (Fig. 4.3a) and filtered data (Fig. 4.3b).

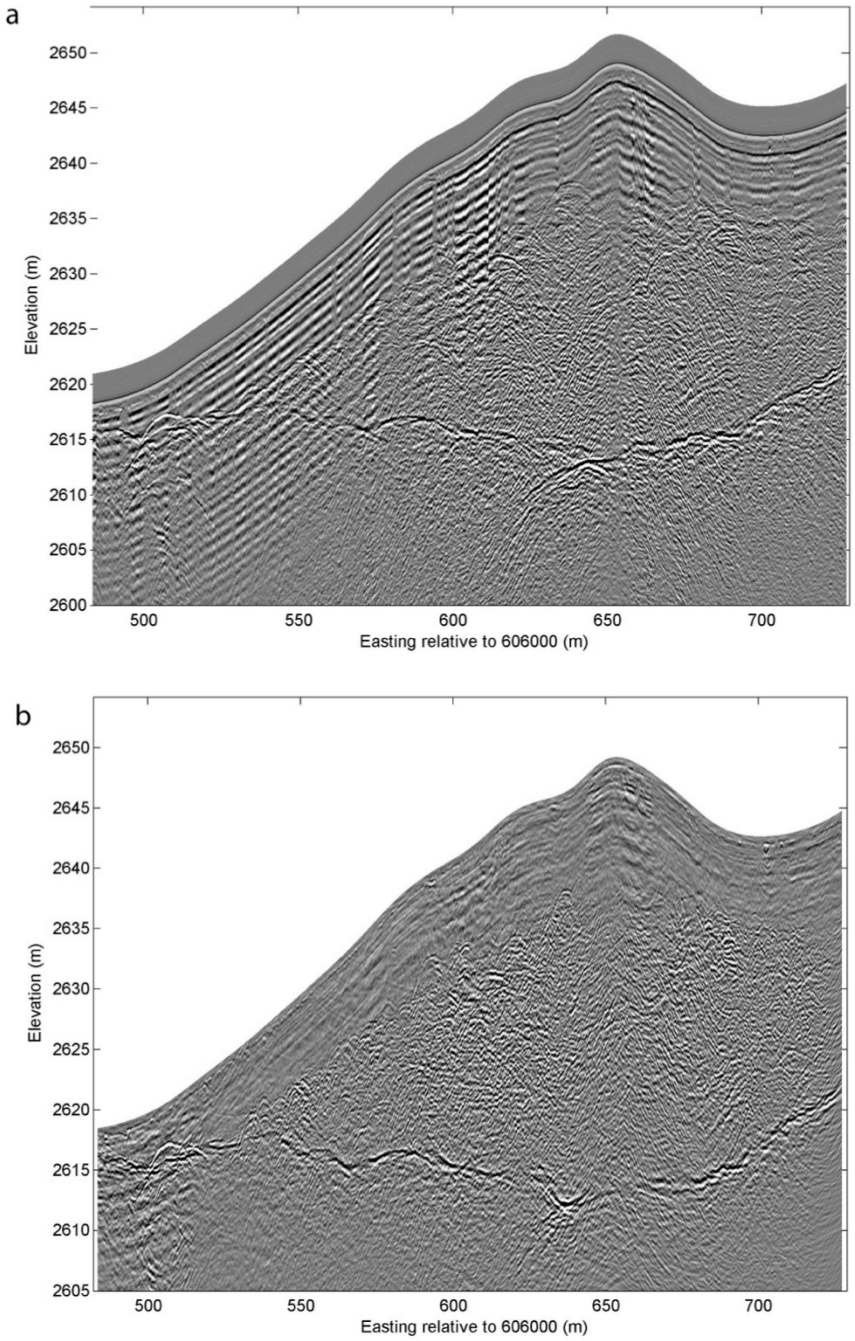

Figure 4.3: Ground-penetrating radar survey profile after dewow, gain and binning but before (a) and after (b) principal component filtering and migration

4.2.6 Migration

In structurally complex ground-penetrating radar surveys, mispositioning of reflectors, modification of the observed depth and loss of resolution can be produced by heterogeneities, dispersion and attenuation effects (Sena, Stoffa and Sen, 2005). Thus using more complex processing is required to obtain a more reliable image of the subsurface in terms of depth, rather than time (Figs. 4.4 and 4.5).

Migration allows refocusing scattered waves to their correct locations thus showing where the reflected energy originated. Migration requires a good knowledge of the velocity distribution in the subsurface – which is not always available – as well as an awareness of the artefacts migration may introduce in the data. Therefore making it an

iterative process between background velocity adjustment and optimized migrated results (Annan, 2001).

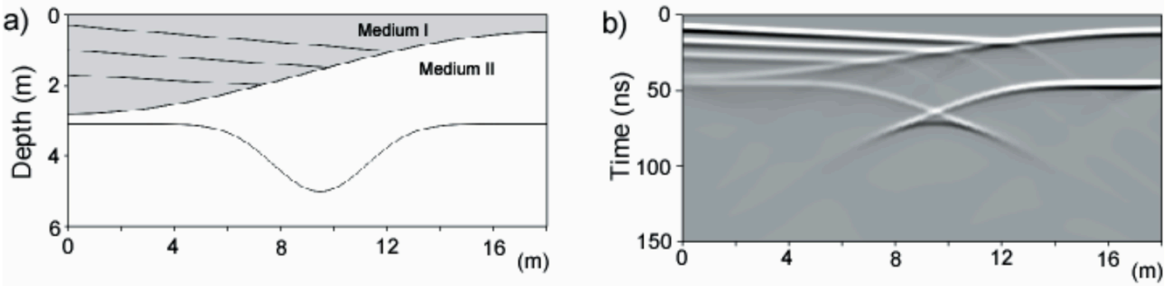

Figure 4.4: A model of the subsurface (a) and simulated unmigrated GPR result (b) for this particular model. Reflectors are mispositioned (Sena, Stoffa and Sen, 2005).

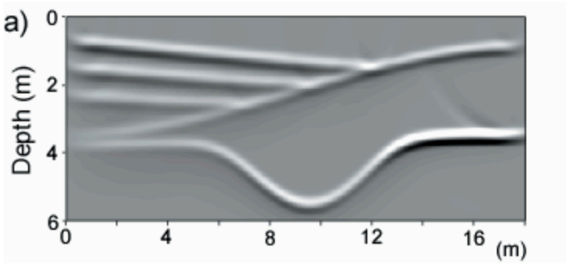

Figure 4.5: Simulated migrated result. Scatterers and reflectors are refocused in their correct position (Sena, Stoffa and Sen, 2005).

For this particular study, an F-K migration method was used. This method performs a post stack migration in the frequency wavenumber domain using the constant velocity method of Stolt (Stolt, 1978). CREWES Project (Margrave and Bancroft, 1996) codes were used to perform F-K migration. Velocity distributions in the subsurface were determined for each profile by fitting diffraction hyperbolas using matGPR software by Andreas Tzanis (Tzanis, 2013) and were comprised between 0.14 m/ns and 0.15 m/ns.

4.2.7 Picking

Picking allows to pull out interesting features of large data set and to display them in a simplified manner with 3D visualization in mind. The main downsides of manual picking are that it is a subjective process and secondly it may oversimplify the reality by giving a false impression of real conditions (Annan, 2001). Automated picking strategies exist to reduce subjectivity, but were not used in this particular study.

Picking was performed on the glacier bed and glacier surface on all profiles as well as the subglacial channel roof and bed.

Picking the glacier bed was relatively straightforward on most profiles as it was clearly visible, however picking the channels turned out to be difficult especially on the most uphill profiles, where outlines of the channels were hard to differentiate from other reflectors. Also given the fact that it is a highly subjective process, performed picking could contain substantial errors, making following processing and modelling significantly inaccurate. It is also important to note that even though all those processing steps are performed to improve the data sets, they do also alter them. Furthermore, ground-penetrating radar only allows to make assumptions on the subsurface conditions, which can only be verified by performing boreholes or by using other digging methods.

5. References

Annan, A. P. (2001). *Ground Penetrating Radar Workshop Notes*. Ontario, Canada: Sensors & Software Inc.

Arnold, N., Richards, K., Willis, I., & Sharp, M. (1998). Initial results from a distributed, physically based model of glacier hydrology. *Hydrological Processes*, *12*, 191–219.

Bamber, J. (1987). Internal reflecting horizons in Spitsbergen glaciers. *Annals of Glaciology*, *9,* 5-10.

Benn, D., Gulley, J., Luckman, A., Adamek, A., & Glowacki, P. S. (2009). Englacial drainage systems formed by hydrologically driven crevasse propagation. *Journal of Glaciology*, *55*(191), 513–523.

Björnsson, H. (1998). Hydrological characteristics of the drainage system beneath a surging glacier. *Nature*, *395*(6704), 771–774.

Brown, J., Harper, J., & Bradford, J. (2009). A radar transparent layer in a temperate valley glacier: Bench Glacier, Alaska. *Earth Surface Processes and Landforms*, *34*(11), 1497–1506. http://doi.org/10.1002/esp.1835

Collins, D. (1989). Seasonal development of subglacial drainage and suspended sediment delivery to melt waters beneath an alpine glacier. *Annals of Glaciology*, *13*, 45–50.

Copland, L., Harbor, J., & Sharp, M. (1997). Borehole video observation of englacial and basal ice conditions in a temperate valley glacier. *Annals of Glaciology*, *24*, 277–282.

Cuffey, K. M., & Paterson, W. S. (2010). *The physics of glaciers* (4th edition). Burlington: Butterworth-Heinemann.

Cutler, P. (1998). Modelling the evolution of subglacial tunnels due to varying water input. *Journal of Glaciology*, *45*(149), 101–111.

Engelhardt, H., Harrison, W. D., & Kamb, B. (1978). Basal sliding and conditions at the glacier bed as revealed by bore-hole photography. *Journal of Glaciology*, *20*(84).

Ferguson, R. (2007). Flow resistance equations for gravel- and boulder-bed streams. *Water Resources Research*, *43*(5). http://doi.org/10.1029/2006WR005422

Fountain, A. G. (1993). Geometry and flow conditions of subglacial water at South Cascade Glacier, Washington State, U.S.A.; an analysis of tracer injections. *Journal of Glaciology*, *39*(131), 143–156.

Fountain, A. G., & Walder, J. S. (1998). Water flow through temperate glaciers. *Reviews of Geophysics*, *36*(3).

Gabbud, C., Micheletti, N., & Lane, S. N. (2015). Lidar measurement of surface melt for a temperate Alpine glacier at the seasonal and hourly scales. *Journal of Glaciology*, *61*(229), 963–974. http://doi.org/10.3189/2015JoG14J226

Gerlitz, K., Knoll, M. D., Cross, G. M., Luzitano, R. D., & Knight, R. (1993). Processing ground penetrating radar data to improve resolution of near-surface targets. In *Symposium on the Application of Geophysics to Environnemental and Engineering Problems* (pp. 561–575). San Diego, USA.

Gordon, S., Sharp, M., Hubbard, B., Smart, C., Ketterling, B., & Willis, I. (1998). Seasonal reorganization of subglacial drainage inferred from measurements in boreholes. *Hydrological Processes*, *12*(1), 105–133.

Gulley, J. D., Grabiec, M., Martin, J. B., Jania, J., Catania, G., & Glowacki, P. (2012a). The effect of discrete recharge by moulins and heterogeneity in flow-path efficiency at glacier beds on subglacial hydrology. *Journal of Glaciology*, *58*(211), 926–940. http://doi.org/10.3189/2012JoG11J189

Gulley, J. D., Spellman, P. D., Covington, M. D., Martin, J. B., Benn, D. I., & Catania, G. (2013). Large values of hydraulic roughness in subglacial conduits during conduit enlargement: implications for modeling conduit evolution. *Earth Surface Processes and Landforms*, *39*(3), 296–310. http://doi.org/10.1002/esp.3447

Gulley, J. D., Walthard, P., Martin, J., Banwell, A. F., Benn, D. I., & Catania, G. (2012b). Conduit roughness and dye-trace breakthrough curves: why slow velocity and high dispersivity may not reflect flow in distributed systems. *Journal of Glaciology*, *58*(211), 915–925. http://doi.org/10.3189/2012JoG11J115

Hock, R. (2005). Glacier melt: a review of processes and their modelling. *Progress in Physical Geography*, *29*(3), 362–391. http://doi.org/10.1191/0309133305pp453ra

Hooke, R. (1984). On the role of mechanical energy in maintaining subglacial water conduits at atmospheric pressure. *Journal of Glaciology*, *30*(105), 180–187.

Hooke, R., Laumann, T., & Kohler, J. (1990). Subglacial water pressures and the shape of subglacial conduits. *Journal of Glaciology*, *36*(122), 67–71.

Hooke, R., Miller, S. B., & Kohler, J. (1988). Character of the englacial and subglacial drainage system in the upper part of the ablation area of Storglaciären, Sweden. *Journal of Glaciology*, *34*(117), 228–231.

Hooke, R., Wold, B., & Hagen, J. O. (1985). Subglacial hydrology and sediment transport at Bondhusbreen, southwest Norway. *Geological Society of America Bulletin*, *96*(3), 388–397.

Hubbard, B., & Nienow, P. (1997). Alpine subglacial hydrology. *Quaternary Science Reviews*, *16*(9), 939–955.

Hubbard, B., Sharp, M., Willis, I. C., Nielsen, M. K., & Smart, C. (1995). Borehole water-level variations and the structure of the subglacial hydrological system of Haut Glacier d'Arolla, Valais, Switzerland. *Journal of Glaciology*, *41*(139), 572–583.

Irvine-Fynn, T. D. L., Moorman, B. J., Williams, J. L. M., & Walter, F. S. A. (2006). Seasonal changes in ground-penetrating radar signature observed at a polythermal glacier, Bylot Island, Canada. *Earth Surface Processes and Landforms*, *31*(7), 892–909. http://doi.org/10.1002/esp.1299

Irving, J., & Knight, R. (2006). Numerical modeling of ground-penetrating radar in 2-D using MATLAB. *Computers & Geosciences*, *32*(9), 1247–1258. http://doi.org/10.1016/j.cageo.2005.11.006

Jania, J., Macheret, Y. Y., Navarro, F. J., Glazovsky, A. F., Vasilenko, E. V., Lapazaran, J., … Piwowar, B. A. (2005). Temporal changes in the radiophysical properties of a polythermal glacier in Spitsbergen. *Annals of Glaciology*, *42*(1), 125–134. http://doi.org/10.3189/172756405781812754

Jania, J., Mochnacki, D., & Gadek, B. (1996). The thermal structure of Hansbreen, a tidewater glacier in southern Spitsbergen, Svalbard. *Polar Research*, *15*(1), 53–66.

Kamb, B. (1987). Glacier surge mechanism based on linked cavity configuration of the basal water conduit system. *Journal of Glaciology*, *92*(9), 9083–9100.

King, E. C., Smith, A. M., Murray, T., & Stuart, G. W. (2008). Glacier-bed characteristics of midtre Lovenbreen, Svalbard, from high-resolution seismic and radar surveying. *Journal of Glaciology*, *54*(184), 145–156.

Kulessa, B., Booth, A. D., Hobbs, A., & Hubbard, A. L. (2008). Automated monitoring of subglacial hydrological processes with ground-penetrating radar (GPR) at high temporal resolution: scope and potential pitfalls. *Geophysical Research Letters*, *35*(24). http://doi.org/10.1029/2008GL035855

Lane, S. N., Bakker, M., Gabbud, C., Micheletti, N., & Saugy, J.-N. (in press). Sediment export, transient landscape response and catchment-scale connectivity following rapid climate warming and Alpine glacier recession. *Geomorphology*.

Liestøl, O. (1967). *Storbreen glacier in Jotunheimen, Norway*. Oslo: Norsk Polarinstitutt.

Lliboutry, L. (1968). General theory of subglacial cavitation and sliding of temperate glaciers. *Journal of Glaciology*, *7*(49), 21–58.

Lliboutry, L. (1983). Modifications to the theory of intraglacial waterways for the case of subglacial ones. *Journal of Glaciology*, *29*(102), 216–226.

Mair, D., Nienow, P., Sharp, M. J., Wohlleben, T., & Willis, I. C. (2002). Influence of subglacial drainage system evolution on glacier surface motion: Haut Glacier d'Arolla, Switzerland. *Journal of Geophysical Research*, *107*(B8). http://doi.org/10.1029/2001JB000514

Mair, D., Willis, I., Fischer, U. H., Hubbard, B., Nienow, P., & Hubbard, A. (2003). Hydrological controls on patterns of surface, internal and basal motion during three"spring events": Haut Glacier d'Arolla, Switzerland. *Journal of Glaciology*, *49*(167), 555–567.

Margrave, G. F., & Bancroft, J. (1996). *CREWES Project* [MATLAB]. University of Calgary.

Murray, T., Stuart, G. W., Fry, M., Gamble, N. H., & Crabtree, M. D. (2000). Englacial water distribution in a temperate glacier from surface and borehole radar velocity analysis. *Journal of Glaciology*, *46*(154), 389–398.

Nienow, P., Sharp, M., & Willis, I. (1996). Temporal Switching between Englacial and Subglacial Drainage Pathways: Dye Tracer Evidence from the Haut Glacier d'Arolla, Switzerland. *Geografiska Annaler. Series A, Physical Geography*, *78*(1), 51. http://doi.org/10.2307/521134

Nienow, P., Sharp, M., & Willis, I. (1998). Seasonal changes in the morphology of the subglacial drainage system, Haut Glacier d'Arolla, Switzerland. *Earth Surface Processes and Landforms*, *23*(9), 825–843.

Nitsche, M., Rickenmann, D., Turowski, J. M., Badoux, A., & Kirchner, J. W. (2011). Evaluation of bedload transport predictions using flow resistance equations to account for macro-roughness in steep mountain streams. *Water Resources Research*, *47*(8).

Nye, J. F. (1976). Water flow in glaciers: jökulhaups, tunnels and veins. *Journal of Glaciology*, *17*(76), 181–207.

Odegard, R., Hagen, J., & Hamran, S.-E. (1996). Comparison of radio-echo sounding (30–1000 MHz) and high-resolution borehole-temperature measurements at Finsterwalderbreen, southern Spitsbergen, Svalbard. *Annals of Glaciology*, *24*(6).

Pälli, A., Moore, J. C., Jania, J., Kolondra, L., & Glowacki, P. (2003). The drainage pattern of Hansbreen and Werenskioldbreen, two polythermal glaciers in Svalbard. *Polar Research*, *22*(2), 355–371.

Rickenmann, D. (1991). Hyperconcentrated flow and sediment transport at steep flow. *Journal of Hydraulic Engineering*, *117*.

Rickenmann, D., & Recking, A. (2011). Evaluation of flow resistance equations using a large field data base. *Water Resources Research*, *47*(7).

Rippin, D., Willis, I., Arnold, N., Hodson, A., Moore, J., Kohler, J., & Björnsson, H. (2003). Changes in geometry and subglacial drainage of Midre Lovénbreen, Svalbard, determined from digital elevation models. *Earth Surface Processes and Landforms*, *28*(3), 273–298. http://doi.org/10.1002/esp.485

Röthlisberger, H. (1972). Water pressure in intra- and subglacial channels. *Journal of Glaciology*, *11*(62), 177–203.

Sena, A. R., Stoffa, P. L., & Sen, M. K. (2005). Migration of Ground Penetrating Radar data in heterogeneous and dispersive media. In *New strategies for European remote sensing: proceedings of the 24th Symposium of the European Association of Remote Sensing Laboratories, Dubrovnik, Croatia, 25-27 May 2004*. Rotterdam: Millpress.

Sharp, M., Richards, K., Willis, I., Arnold, N., Nienow, P., Lawson, W., & Tison, J.-L. (1993). Geometry, bed topography and drainage system structure of the Haut Glacier d'Arolla, Switzerland. *Earth Surface Processes and Landforms*, *18*(6), 557–571.

Shreve, R. L. (1972). Movement of water in glaciers. *Journal of Glaciology*, *11*(62), 205–214.

Stolt, R. H. (1978). Migration by Fourier transform. *Geophysics*, *43*(1).

Stuart, G., Murray, T., Gamble, N., Hayes, K., & Hodson, A. (2003). Characterization of englacial channels by ground-penetrating radar: An example from austre Brøggerbreen, Svalbard. *Journal of Geophysical Research*, *108*(B11). http://doi.org/10.1029/2003JB002435

Swift, D. A., Nienow, P. W., & Hoey, T. B. (2005a). Basal sediment evacuation by subglacial meltwater: suspended sediment transport from Haut Glacier d'Arolla, Switzerland. *Earth Surface Processes and Landforms*, *30*(7), 867–883. http://doi.org/10.1002/esp.1197

Swift, D. A., Nienow, P. W., Hoey, T. B., & Mair, D. W. F. (2005b). Seasonal evolution of runoff from Haut Glacier d'Arolla, Switzerland and implications for glacial geomorphic processes. *Journal of Hydrology*, *309*(1-4), 133–148. http://doi.org/10.1016/j.jhydrol.2004.11.016

Tzanis, A. (2013). MATGPR (Version 3) [MATLAB]. Department of Geophysics, University of Athens, Greece.

Vincent, C., Descloitres, M., Garambois, S., Legchenko, A., Guyard, H., & Gilbert, A. (2012). Detection of a subglacial lake in Glacier de Tête Rousse (Mont Blanc area, France). *Journal of Glaciology*, *58*(211), 866–878. http://doi.org/10.3189/2012JoG11J179

Walder, J. S. (2010). Rothlisberger channel theory: its origins and consequences. *Journal of Glaciology*, *56*(200), 1079–1086.

Walder, J. S., & Fowler, A. (1994). Channelized subglacial drainage over a deformable bed. *Journal of Glaciology*, *40*(134), 3–15.

Weertman, J. (1983). Stability of sheet water flow under a glacier. *Journal of Glaciology*, *29*(103).

Welch, B. ., Pfeffer, W. T., Harper, J. T., & Humphrey, N. F. (1998). Mapping subglacial surfaces of temperate valley glaciers by two- pass migration of radio-echo sounding survey data. *Journal of Glaciology*, *44*(146).

Willis, I., Lawson, W., Owens, I., Jacobel, B., & Autridge, J. (2009). Subglacial drainage system structure and morphology of Brewster Glacier, New Zealand. *Hydrological Processes*, *23*(3), 384–396. http://doi.org/10.1002/hyp.7146

Zryd, A. (2001). *Les Glaciers*. Saint Maurice: Editions Pillet.